LAPPEENRANTA
UNIVERSITY OF TECHNOLOGY

Alexander Lashkul

QUANTUM TRANSPORT PHENOMENA AND SHALLOW IMPURITY STATES IN CdSb

Thesis for the degree of Doctor of Philosophy to be presented with due permission for public examination and criticism in the Auditorium 1383 at Lappeenranta University of Technology, Lappeenranta, Finland on the 17th of December, 2007, at noon.

Acta Universitatis
Lappeenrantaensis
295

Supervisor Prof. Erkki Lähderanta
Department of Mathematics and Physics
Lappeenranta University of Technology,
Lappeenranta, Finland

Reviewers Prof. Michel Goiran
Laboratoire **N**ational des **C**hamps **M**agnétiques **P**ulsés
(L N C M P)
Toulouse, France

Prof. Pekka Ruuskanen
Tampere University of Technology,
Tampere, Finland

Opponent Prof. Nikita S. Averkiev
Ioffe Physico-Technical Institute, Russian Academy of Sciences,
St. Petersburg, Russia

ISBN 978-952-214-506-2
ISBN 978-952-214-507-9 (PDF)
ISSN 1456-4491

Lappeenrannan teknillinen yliopisto
Digipaino 2007

To my wife

Abstract

Alexander Lashkul

Quantum transport phenomena and shallow impurity states in CdSb

Lappeenranta 2007

77 p.

Acta Universitatis Lappeenrantaensis 295

Diss. Lappeenranta University of Technology

ISBN 978-952-214-506-2, ISBN 978-952-214-507-9 (PDF), ISSN 1456-4491

This work is dedicated to investigation of the energy spectrum of one of the most anisotropic narrow-gap semiconductors, CdSb. At the beginning of the present studies even the model of its energy band structure was not clear. Measurements of galvanomagnetic effects in wide temperature range (1.6 – 300 K) and in magnetic fields up to 30 T were chosen for clarifying of the energy spectrum in the intentionally undoped CdSb single crystals and doped with shallow impurities (In, Ag).

Detection of the Shubnikov – de Haas oscillations allowed estimating the fundamental energy spectrum parameters. The shapes of the Fermi surfaces of electrons (sphere) and holes (ellipsoid), the number of the equivalent extremums for valence band (2) and their positions in the Brillouin zone were determined for the first time in this work. Also anisotropy coefficients, components of the tensor of effective masses of carriers, effective masses of density of states, nonparabolicity of the conduction and valence bands, *g*-factor and its anisotropy for n- and p-CdSb were estimated for the first time during these studies. All the results obtained are compared with the cyclotron resonance data and the corresponding theoretical calculations for p-CdSb. This is basic information for the analyses of the complex transport properties of CdSb and for working out the energy spectrum model of the shallow energy levels of defects and impurities in this semiconductor.

It was found out existence of different mechanisms of hopping conductivity in the presence of metal – insulator transition induced by magnetic field in n- and p-CdSb. Quite unusual feature opened in CdSb is that different types of hopping conductivity may take place in the same crystal depending on temperature, magnetic field or even orientation of crystal in magnetic field.

Transport properties of undoped p-CdSb samples show that the anisotropy of the resistivity in weak and strong magnetic fields is determined completely by the anisotropy of the effective mass of the holes. Temperature and magnetic field dependence of the Hall coefficient and magnetoresistance is attributed to presence of two groups of holes with different concentrations and mobilities. The analysis demonstrates that below $T_{cr} \sim$ 20 K and down to ~ 6 – 7 K the low-mobile carriers are itinerant holes with energy $E_2 \approx$ 6 meV. The high-mobile carriers, at all temperatures $T < T_{cr}$, are holes activated thermally from a deeper acceptor band to itinerant states of a shallower acceptor band with energy $E_1 \approx 3$ meV. Analysis of temperature dependences of mobilities confirms the existence of the heavy-hole band or a non-equivalent maximum and two equivalent maxima of the light-hole valence band.

Galvanomagnetic effects in n-CdSb reveal the existence of two groups of carriers. These are the electrons of a single minimum in isotropic conduction band and the itinerant electrons of the narrow impurity band, having at low temperatures the energies above the bottom of the conduction band. It is found that above this impurity band exists second impurity band of only localized states and the energy of both impurity bands depend on temperature so that they sink into the band gap when temperature is increased. The bands are splitted by the spin, and in strong magnetic fields the energy difference between them decreases and redistribution of the electrons between the two impurity bands takes place.

Mobility of the conduction band carriers demonstrates that scattering in n-CdSb at low temperatures is strongly anisotropic. This is because of domination from scattering on the neutral impurity centers and increasing of the contribution to mobility from scattering by acoustic phonons when temperature increases. Metallic conductivity in zero or weak magnetic field is changed to activated conductivity with increasing of magnetic field. This exhibits a metal-insulator transition (MIT) induced by the magnetic field due to shift of the Fermi level from the interval of extended states to that of the localized states of the electron spectrum near the edge of the conduction band. The Mott variable-range hopping conductivity is observed in the low- and high-field intervals on the insulating side of the MIT. The results yield information about the density of states, the localization radius of the resonant impurity band with completely localized states and about the donor band. In high magnetic fields this band is separated from the conduction band and lies below the resonant impurity bands.

Keywords: Semiconductors, energy band structure, electrical conductivity, transport and quantum transport properties, shallow impurity states, hopping conductivity.

UDC 544.034.7 : 544.225.2 : 539.219.1

Acknowledgements

This work was carried out at the Department of Mathematics and Physics of Lappeenranta University of Technology, Lappeenranta, Finland, the Wihuri Physical Laboratory at the Department of Physics, University of Turku, Turku, Finland, the Ioffe Institute of Russian Academy of Sciences, St. Petersburg, Russia, and Institute of Applied Physics of Moldavian Academy of Sciences, Kishinev, Moldova.

I would like to express my sincere gratitude to my supervisor Prof. Erkki Lähderanta for constant help, care and attention to my activities and for the opportunity to complete this work. Special gratitude is to Prof. Reino Laiho for providing me good conditions for my work in his research group and for always extremely helpful discussions and collaboration.

I wish to tender thanks to Prof. Robert Parfeniev and Prof. Ernest Arushanov for their patient teaching, guiding and support during the fulfilling of the first part of my work. All other co-authors, especially V. V. Sologub, K. G. Lisunov, V. I. Pruglo, M. O. Safonchik and M. A. Shakhov are greatly acknowledged for their experimental and theoretical contributions.

I express my gratitude to the staff of the Wihuri Physical laboratory and helium-liquefying group for constructive, helpful and pleasant atmosphere.

Prof. Michel Goiran and Prof. Pekka Ruuskanen are acknowledged for reviewing the thesis. “Jenny and Antti Wihuri Foundation”, Finland and “Tekniikan Tutkimusinstituutti”, Vaasa, Finland are acknowledged for financial support.

Finally, I wish to thank my beloved wife Tatiana for her love, care and patience during these years and my children Alexander and Maria for substantial help and support during the book preparation and the whole work in general.

Lappeenranta, October 2007

Alexander Lashkul

Contents

List of publications

This thesis is based on the experimental work carried out during the years 1981–1982 and 2004–2007. The thesis consists of an introductory part and the following publications:

Publication 1. E. K. Arushanov, A. V. Lashkul, V. I. Pruglo, S.I. Radautsan, V. V. Sologub, Shubnikov- de Haas oscillations in p-CdSb, Doklady Akademii Nauk SSSR **263**, 1, 71–73 (1982), (in Russian); Sov. Phys. Doklady (USA) **27**, 3, 212–3 (1982).

Publication 2. E. K. Arushanov, A. V. Lashkul, V. I. Pruglo, S.I. Radautsan, V. V. Sologub, Shubnikov–de Haas oscillations in n-CdSb, Doklady Akademii Nauk SSSR **263**, 5, 1112–14 (1982), (in Russian); Sov. Phys. Doklady (USA) **27**, 4, 320–321 (1982).

Publication 3. R. Laiho, A. V. Lashkul, K. G. Lisunov, E. Lähderanta, M. O. Safonchik and M. A. Shakhov, Observation of the anisotropic hopping conductivity of p-CdSb in a magnetic field, J. Phys.: Condens. Matter **16,** 333–342 (2004).

Publication 4. R. Laiho, A. V. Lashkul, K. G. Lisunov, E. Lähderanta, M. O. Safonchik and M. A. Shakhov, Hall effect and band structure of p-CdSb in strong magnetic field, Semicond. Sci. Technol. **19,** 602–609 (2004).

Publication 5. R. Laiho, A. V. Lashkul, K. G. Lisunov, E. Lähderanta, M. O. Safonchik, M. A. Shakhov, The Hall effect and electron energy spectrum near the conduction band edge of n-CdSb in magnetic fields up to 25 T, Semicond. Sci. Technol. **21**, 918–927 (2006).

Publication 6. R. Laiho, A. V. Lashkul, K. G. Lisunov, E. Lähderanta, M. O. Safonchik, M. A. Shakhov, Metal-insulator transition and variable-range hopping conductivity of n-CdSb in magnetic field, J. Physics and Chemistry of Solids, **68,** 272–279 (2007)

Publications are presented in the chronological order. The authors are written in the alphabetical order.

LIST OF SYMBOLS AND ABREVIATIONS

SYMBOLS

$\hbar$	the Plank constant
^0C	Celsius degree (temperature)
Å	Ångstrom (distance)
$a^*(a_i, a_{0i})$	mean localization radius in hopping conductivity model
a, b, c	lattice constants
A_{Ti}	amplitude of the Shubnikov–de Haas oscillation at temperature T_i
B	magnetic field
B_c, B_{cr}	crossover and critical magnetic field in hopping conductivity model, respectively
Cd, Sb, In, Ag, Te, Ga	elements of the Periodic table
C_{ii}	elastic module
$C_{ij}(S_{ij})$	anisotropy coefficients in hopping conductivity model
cos	cosine
e	charge of electron
E, ε	energy
E_F	the Fermi energy
E_g	forbidden energy gap
E_i	ionization energy of impurity level
eV	electron-volt (energy)
g	factor of spin split of energy levels of charge carriers in magnetic field
$g(E_F)$	density of states on the Fermi level
I	electrical current
K	Kelvin degree (temperature)
k, k_i	wave vector and components of wave vector, respectively
k_B	the Boltzman constant
K_{Fi}	linear dimensions in k-space
K_i	anisotropy coefficient
l, d	distance
M	integer
$m, cm, \mu m, nm$	meter, centimeter, micrometer, nanometer
m_0	mass of free electron
m_a, m_b, m_c	components of effective mass tensor of charge carriers
m_c	cyclotron mass of charge carrier
m_n, m_p	effective mass of density of states of electrons and holes, respectively
$ms, \mu s$	millisecond, microsecond (time)
N	number of equivalent energy band extrema
N	Newton (force)
n, p	concentration of electrons and holes, respectively
$N_i(N_A, N_D)$	concentration of impurity
n_i, p_i, μ_i	concentrations and mobilities of charge carriers in different energy sub-bands, respectively
N_m	quantum number of the Landau level
$p(n)_{Hall}$	concentration of charge carriers estimated from the Hall effect
$p(n)_{SdH}$	concentration of charge carriers estimated from the Shubnikov–de Haas effect
P_{SdH}	period of the Shubnikov - de Haas oscillations
R_0, R_∞	The Hall coefficient in zero and infinite magnetic field

R_H	the Hall constant
S, S_m	square and square of the extremal cross of the Fermi surface, respectively
sh	hyperbolic sinus
T	Tesla (magnetic field)
T	temperature (K)
T_0	characteristic temperature in hopping conductivity model
$T_{D\mu}$	the Dingle temperature estimated from the Hall effect
T_D,	the Dingle temperature estimated from the Shubnikov - de Haas effect
V	voltage
α_i	directory cosines
β	temperature coefficient of position of energy sub-band
μ, μ_i	mobility and components of the mobility tensor of free carriers, respectively
ρ_{xx}, ρ_{zz}, ρ_{xy}	transverse, longitudinal and the Hall resistivity in magnetic field, respectively
σ_{cl}, σ_{xx}, σ_{zz},	classical, transverse, longitudinal, the Hall and specific conductivity in magnetic
σ_{xy}, σ	field, respectively
τ	relaxation time
θ	angle
ω_c	cyclotron frequency

ACHRONYMS

CB, VB, IB	conduction, valence and impurity band, respectively
DOS	density of states
LL	the Landau levels
MIT	metal-insulator transition
MR	magnetoresistance
NNH	nearest-neighbor-hopping
SdH	Shubnikov–de Haas
SE	Shklovsky–Efros
VRH	variable-range-hopping

1 Introduction

1.1 Main physical and transport properties of Cadmium Antimonide.

Cadmium Antimonide is a semiconductor from the $A^{II}B^{V}$ group. In the Cd-Sb system, CdSb is the only stable compound with the melting temperature 456 ^{o}C [1] and with the orthorhombic crystal structure D^{15}_{2h}, which is presented in Fig. 1.1.1. The parameters of unit cell, which contains 16 atoms, are a = 6.471 Å, b = 8.253 Å, c = 8.526 Å and distances between atoms are {Cd – Cd} = 2.99 Å; {Sb – Sb} = 2.81 Å; {Cd – Sb} = 2.80 Å; 2.81 Å and 2.91 Å [2].

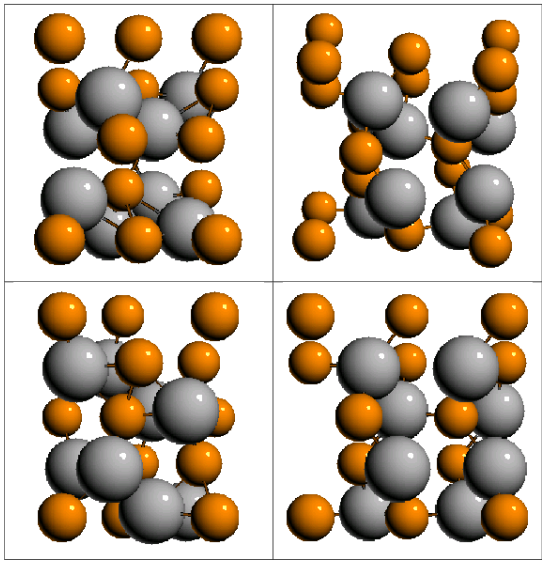

Fig. 1.1.1. Crystal structure of Cadmium Antimonide from several perspectives [2]. Small and large spheres represent Cd and Sb atoms, respectively.

The nature of chemical bonds between atoms in the CdSb crystal lattice was investigated in [2, 3 and 4–6]. Conclusion about the predominant covalent character of chemical bonding in CdSb was independently obtained in [2], [8] and [9]. This is confirmed by the investigation of the mechanical properties of CdSb in [10].

The elastic modules of CdSb were estimated from the speed of ultrasonic waves [11] along the main crystallographic directions and are equal (in N/m^2), and correspondingly

$C_{11} = 7.97 \cdot 10^{10}$; $C_{44} = 1.26 \cdot 10^{10}$; $C_{12} = 2.2 \cdot 10^{10}$;

$C_{22} = 9.5 \cdot 10^{10}$; $C_{55} = 2.98 \cdot 10^{10}$; $C_{13} = 1.2 \cdot 10^{10}$;

$C_{33} = 8.4 \cdot 10^{10}$; $C_{66} = 1.88 \cdot 10^{10}$; $C_{23} = 1.6 \cdot 10^{10}$.

The crystals of CdSb can be prepared as an n- and p-type conductivity depending on the doping impurity; however, an intentionally undoped material has a p-type conductivity because of the intrinsic defects associated with the Cd vacancies [2]. The type of conductivity changes from p- to n-type when doping CdSb by the elements from III and VI groups of the periodic table. During doping, the elements from the groups I and III substitute Cd atoms and act as acceptors, but the elements from the groups IV and VI substitute Sb atoms and act as donors [12, 13]. It is possible to change the type of CdSb conductivity by adding Zn and Pb [7] from the groups II and IV. The most usual acceptor impurity used for CdSb is Ag, which forms a shallow acceptor level [14], and the most usual donor impurity is In with a shallow donor level [11]. The ionization energy of these impurity levels is very small, and they are completely ionized even at 2 K [11, 15, 16]. The conclusion made in [11] claims that in a material heavily doped by Ag or In, the ionization energy is equal to zero. In the intentionally undoped p-CdSb, there exists an acceptor impurity band at the distance of E_i = 3.2 meV and discrete energy levels at the distance of E_i = 6.1 meV from the top of the valence band [15]. These data are in a good agreement with the results of [15], where the measurements of the temperature dependences of electrical conductivity and the Hall coefficient gave a value of E_i = 5 - 8 meV. All the mechanical and electrical properties of CdSb are quite anisotropic, which was noted in the very first investigations of this material [12, 4–6, 18, 19]. The solid-state theory predicts three independent components of the tensors for the Hall coefficient R_H and the electrical conductivity σ in this material [4]. The experimental studies of R_H and σ temperature dependences in undoped crystals in 2–100 K [15], 77–400 K [12, 18] and 2.2–400 K [11,16] temperature ranges showed that at low temperatures, the conductivity decreases with increasing the temperature, $R_H > 0$ and it does not depend on the temperature. Intrinsic conductivity starts at 270 K. The temperature dependences of the conductivity tensor components are similar and $\sigma_{[001]} > \sigma_{[100]} > \sigma_{[010]}$. Such a ratio between components was confirmed in practice in all the following investigations [4, 5, 11, 15, 16].

The ratio between the mobility tensor components μ_i is similar to the conductivity components: $\mu_{[001]} > \mu_{[100]} > \mu_{[010]}$ [4, 5, 11, 15, 16]. At low temperatures, the mobility with temperature follows the law $\mu_i \sim T^{3/2}$ [5, 6]. In [11, 16], it was assumed that at high temperatures, the scattering takes place on the optical phonons, but at low temperatures, on the impurity ions, while a part of the scattering on the impurity grows with the increasing of the concentration of holes. It was found out that the Hall coefficient R_H is practically isotropic in the doped and undoped samples [11, 16, 19, 21]. The temperature, magnetic field and angle dependences of the components of the magnetoresistance tensor M^k_i (electric current || i; magnetic field || k; i (k) ≤ 3, where [100] ≡ 1; [010] ≡ 2; [001] ≡ 3) were investigated in

undoped [28, 47, 55, 58], weakly doped [11, 19, 22] and heavily doped [11, 22] CdSb samples with an n- and p-type of conductivity. The temperature and orientation dependences of magnetoresistance components of the p-type samples on the magnetic field were investigated in magnetic fields up to 1 T. Increasing of the components M^k_i with decreasing the temperature was noted in [6, 19, 22]. The temperature dependence of the transverse coefficients M^2_1 and M^2_3 obeys the law $T^{-3.3}$, but longitudinal M^2_2 obeys the law T^{-2} [19]. The angle dependences of M^k_i are periodic with the period of 180° [6, 19, 22].

In the study, the n-type conductivity is not investigated in such detail as the p-type. The anisotropy of the electrical conductivity and the Hall coefficient in n-CdSb is small ($\mu_{1n} : \mu_{2n} : \mu_{3n}$ = 2.7 : 1.7 : 2.2 at 250 K) in comparison with the p-type [6, 11, 19, 22]. Only in [11], a considerable anisotropy of σ was observed in the n-type material doped with Te and In in the 170 K–200 K temperature range. These results were explained in [17] by the non-equivalent distribution of impurities (Te, In, Ge, Se,Ga) in the different quenching planes of crystal. The results for homogeneous samples were reported for the first time in [11, 16]; in these studies, n-type samples that were doped with In were investigated, the concentration of electrons being in the range of $1.5 \cdot 10^{16}$–$1.5 \cdot 10^{18}$ cm^{-3}. Below the bottom of the conductivity band, doping of CdSb with In produces shallow donor levels, which merge with the band edge in heavily doped n-CdSb leading to the degeneracy of electron gas near liquid helium temperatures [11].

The temperature dependence of thermoelectric power in the undoped CdSb was investigated in [4, 6, 11, 12, 16]. At low temperatures, thermoelectric power is practically isotropic up to 270 K. Anisotropy starts to increase dramatically at higher temperatures to such extent that the thermoelectric voltage even changes its sign from positive to negative with increasing temperature, when the temperature gradient is parallel to [010]. In n-CdSb crystals doped with In, Te [12] and Ga [12, 23], anomalies were observed in the temperature dependences of thermoelectric power at low doping levels. However, when the concentration of electrons exceeds 10^{17} cm^{-3} in the case of Te [19] and $5 \cdot 10^{17}$ cm^{-3} in the case of In [23], the sign of thermoelectric voltage remains negative in the whole temperature range.

Lattice excitations in CdSb were studied in depth in [85] at 2 K on a undoped p-CdSb sample by the Fourier Transform Spectroscopy technique in the wave number region 30 to 300 cm^{-1} in a magnetic field up to 18 T. It was shown that three absorption bands dominate the spectra; first, it was proved that the contribution of electronic excitation in the IR and Raman spectra is weak or absent, and second, that the dynamical properties of CdSb are closely related to the InSb ones.

1.2 Models of the energy band structure of Cadmium Antimonide

Over the past several years, numerous experimental and theoretical studies have focused on the energy band structure of Cadmium Antimonide. The main parameter of any semiconductor, the forbidden energy gap E_g, is estimated in CdSb by electrical, optical and photoelectrical measurements. To our knowledge, E_g was estimated for the first time as 0.58 eV in [12] and 0.57 eV in [4] (both values are for 0 K). These estimates were based on calculated from the temperature dependence of the conductivity assuming scattering of the carriers on the acoustic phonons and the equality of mobilities of electrons and holes. The temperature coefficient α of $E_g = \alpha T$ estimated in [27] and equal to $-3.56 \cdot 10^{-4}$ eV/K helps to understand the results obtained in [11], where E_g at 300 K was found to be close to (0.46 ± 0.01) eV. The value of the optical E_g estimated at 300 K under the illumination by non-polarized light turned out to be 0.456 eV [18] and 0.45 eV [28]. The experiments with polarized light performed in [20, 29, 30] gave an E_g value of 0.43 eV at 300 K and 0.5 eV at 0 K. The analyses of the decay of the long wave photoconductivity edge carried out in [27] led to an E_g value equal to $(0.535–3.56 \cdot 10^{-4}\ T)$ eV that correlates well with [20, 29, 30]. Finally, the results presented above allow to conclude that at 0 K, the thermal E_g in CdSb is equal to (0.575 ± 0.005) eV, and the optical E_g is equal to (0.518 ± 0.018) eV.

The effective masses of the density of states (DOS) m_p/m_0 and the components of the tensor m_{ii}/m_0 of the effective masses were estimated in CdSb by studies of cyclotron resonance [31, 32], thermoelectric power [11, 12, 14, 23, 28], magnetic susceptibility [33], IR plasma reflection [34, 35] and galvanomagnetic effects [13, 22]. Determination of the DOS effective mass m_p/m_0 from thermoelectric power is possible when the mechanism of scattering is known; this was performed for the valence band in undoped crystals at 100 K. The values obtained for m_p/m_0 lie in the range of 0.2–0.5 in [13, 28], 0.3 in [14] and 0.4–0.5 in [11]. Also the value of $m_p/m_0 = 0.37$ was calculated from the temperature dependences of the Hall coefficient and electrical conductivity [13].

The effective mass of the DOS for the conduction band m_n/m_0 in CdSb doped with In (concentration of electrons $5 \cdot 10^{17}$ cm^{-3}) [23] and with 0.1% Te [11] was estimated at 100 K and is equal to 0.49 and 0.6–0.7, respectively. The effective mass of the free carriers in p-CdSb was measured with high accuracy applying cyclotron resonance studies [32], yet the sign of the carriers in the resonance was not defined. In spite of the fact that the material was of p-type, the resonance itself took place only under the illumination of the sample by light with the energy higher than the forbidden energy gap, which allows to assume that it was question of electrons. It was found out that the Fermi surface of these carriers has a shape of

ellipsoid of revolution with the longitudinal and transverse effective masses 0.159 m_0 and 0.140 m_0, respectively.

The components of the effective mass tensor of holes $m_a/m_0 = 0.48$, $m_b/m_0 = 0.44$ and $m_c/m_0 = 0.17$ were measured by magnetic susceptibility [33] and magnetoresistance [22] assuming that the Fermi surfaces of holes are ellipsoids and their main axes are parallel to the main crystallographic directions of CdSb crystal lattice **a** [100], **b** [010] and **c** [001]. Analyzing the mobility of holes in the heavily doped crystals [21] gave the values of 0.3 and 0.15 for m_b/m_0 and for m_c/m_0, respectively.

The estimation of the effective masses of holes was carried out during the studies of the IR plasma reflection of CdSb [34, 36]. In [34], the measurements were performed in the wavelength range of 2–25 μm for the hole concentrations of $1 \cdot 10^{18}$–$2 \cdot 10^{19}$ cm^{-3}, and the dependence of m_i/m_0 vs. the concentration of holes was detected. The effective mass values of holes for the investigated samples are in the range of $m_a/m_0 = 0.02$–0.33, $m_b/m_0 = 0.05$–0.48 and $m_c/m_0 = 0.05$–0.13. Such large changes in the concentration indicate high non-parabolicity of the valence band in CdSb, being comparable with the non-parabolicity of InSb and InAs.

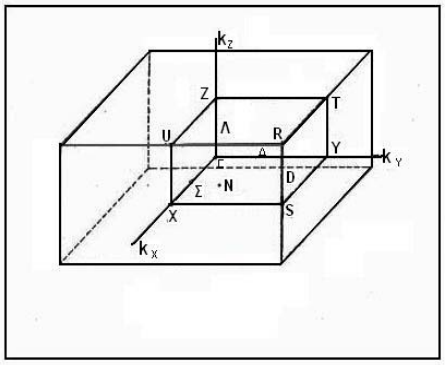

Fig. 1.2.1. Symmetry points of the first Brillouin zone of Cadmium Antimonide.

The results for CdSb crystals [36], with the concentration of holes of $7 \cdot 10^{18}$–$3 \cdot 10^{19}$ cm^{-3} using the wavelengths 3–30 μm at 85 K, are for $m_a/m_0 = 0.23$; $m_b/m_0 = 0.38$ and $m_c/m_0 = 0.12$, with a weak temperature dependence. Based on the data about the relaxation times of holes, it was concluded that the preferable mechanism of the scattering of holes at low temperatures is the scattering on the ionized impurities [36]. Attempts to analyze the energy band structure of CdSb have been undertaken in numerous publications [19, 24–26, 35, 37–40]. The possible variants of location of the extrema of the bands were analyzed based on the theoretical calculations and experimental data in [19, 24, 25, 35, 37–39]. The conclusions on

the location of the valence band maximum in the centre (one valley) and of the conductivity band minimum in the point ***R*** of the Brillouin zone are made in [24, 26] on the basis of the similarity of chemical bonds in Ge, ZnSb and CdSb; this was experimentally proved for ZnSb in [40]. The investigations of the polarized light absorption and reflection [35] show the special role of the crystallographic direction [100]. It was proposed in [35] to place the minimum of the conductivity band to the point ***N*** (4 equivalent valleys) and the maximum of the valence band to point Σ (2 valleys) of the Brillouin zone. One type of holes and electrons was detected in the valence and conductivity bands, respectively. The valence band structure of CdSb was analyzed in [19] applying the results of galvanomagnetic effects. The obtained results can be explained in the frames of the 4-valley-model of the Fermi surface of holes when the axes of ellipsoids are not parallel to the main crystallographic axes of the crystal and have an angle of 10^{o} with them. It was mentioned that the existence of two types of holes in the valence band of CdSb is probable.

The experimental results of the piezoresistance [37] and absorption edge of CdSb in the range of indirect transitions [25] lead to a model of an energy band structure with three nonequivalent maxima of the valence band located in the Γ point of the Brillouin zone and the conductivity band with three nonequivalent minima located in Δ, Σ and Λ points of the Brillouin zone (see Fig. 1.2.1). Taking into account the peculiarity of [100] direction, it was proposed to consider ellipsoids in Δ and Λ points to be equivalent, and in point Σ to be different from the (??) ellipsoid of revolution [37]. However, it was shown in [25] that this may be considered only a zero approximation, and in general, all the three conductivity bands are not equivalent.

The theoretical calculations of the energy band structure of CdSb have been performed applying an empirical pseudo potential method in the single space group representation in [38, 39]. The calculated band structures show that both the bottom of the conduction band and the top of the valence band are on the symmetry line [100]. It is found that the lowest energy gap of 0.49 eV is indirect one from Σ_4 to Σ_1 on this line.

The maxima of the valence band lie on [100] axis in the point of *k*-space with the coordinates (0.8 π/a; 0; 0) and follow the Σ_4 symmetry (2 anisotropic ellipsoids of general shape). Also the conduction band minima are located on [100] axis in the point (0.5 π/a; 0, 0) and follow the Σ_1 symmetry (2 equivalent spheres). In this model of the energy band structure, it is shown that in the conduction band, there may exist one more sub-band with Δ symmetry 50 meV higher than the main minimum. The calculated effective masses of electrons and holes are practically isotropic for electrons and have a ratio $m_{p1} : m_{p2} : m_{p3}$ = 1.6 : 3.35 : 1.00 for holes.

1.3 Motivation of the present work

Motivation of the present work is clear because the review of the data presented above shows that even the energy band structure of CdSb was a subject of extensive discussion before this investigation. Numerous variants were proposed for the energy band structure of this material: one-, two-, four- and six-valley models for the valence band and two- and four- valley models for the conduction band. The mechanisms of conductivity in this material were not defined at all in spite of the large number of publications.

The lack of such information makes the practical use of CdSb impossible as a prospective material for spintronics, which was found recently in our experiments [69]. Investigation of transport properties of CdSb at low temperatures in high magnetic fields is a powerful instrument to find answers to the questions that concern the energy band structure and conductivity mechanisms in this semiconductor. The results of the present investigations raised new interest in the energy band structure of CdSb, where a higher level of more accurate calculations may be achieved [39, 82–87].

2. Theoretical background and experimental procedure

2.1 Quantum galvanomagnetic effects in semiconductors

The energy spectrum of charge carriers in the solid state is quantized when applying a strong magnetic field. Therefore, the DOS of charge carriers demonstrates oscillating behavior vs. energy with changing of the magnetic field. Landau described this phenomenon in the frame of quantum mechanics [41], which presents the nature of quantization for the DOS of charge carriers within the bounds of the isotropic quadratic law of dispersion of free electrons. The analysis shows that energy in a magnetic field can be described by the expression:

$$\varepsilon_{Nmkykz} = (N_m + 1/2)\hbar\omega_c + \frac{\hbar^2 k^2{}_z}{2m_c}, \qquad (2.1.1)$$

where the electron frequency $\omega_c = eB/m_c$, m_c is the cyclotron mass of electron (or hole), N_m is an integer and k_i is the charge carrier wave vector component along the axis $\boldsymbol{i}$ ($\boldsymbol{i}$ = $\boldsymbol{y}$ or z), and the magnetic field is parallel to axis $\vec{z}$. The first part in Eq. 2.1.1 is the discrete variable energy of electron (hole) motion in the plane perpendicular to the direction of the magnetic field. The second term is the energy of continuous electron (hole) motion along $\vec{z}$-axis. Thus, the three-dimensional zone with quasicontinuous distribution of energy levels in $\boldsymbol{k}$-space splits to a number of one-dimensional magnetic sub-bands or a Landau level because of the energy quantization of the orbital motion of the charge carriers in the plane perpendicular to the direction of the magnetic field. The distance between the energy sub- bands is equal to the cyclotron energy $\hbar\omega_c$. The level with $N_m = 0$ is situated $\frac{\hbar\omega_c}{2}$ above the conduction band without magnetic field (see Fig. 2.1.1).

The distribution *ρ(E)* of the DOS of the charge carriers in the quantizing magnetic field starts to depend on the magnetic field:

$$\rho(E) = \frac{m^{3/2}}{\sqrt{2}\pi^2\hbar^3}\frac{\hbar\omega_c}{2}\sum_{N_m=0}^{N_{\max}}[E - (N_m + 1/2)\hbar\omega_c]^{-1/2}. \qquad (2.1.2)$$

The discontinuous character of the function *ρ(E)* close to the points $E = (N_m + 1/2)\hbar\omega_c$ leads to non-monotonic peculiarities of the transport properties (in particular of the magnetoresistance) because the DOS turn to infinite in the vicinity of the bottom of each Landau sub-band (see Fig. 2.1.1).

The Fermi energy E_F depends on the magnetic field and is connected to the zero field Fermi energy

$$E_{F_0} = \left(\hbar^2 \big/ 2m\right) \cdot \left(3\pi^2 n\right)^{2/3} \tag{2.1.3}$$

by

$$\frac{2}{3}\left(\frac{E_{F_0}}{\hbar\omega_c}\right) = \sum_{N_m=0}^{N_{\max}} [E - (N_m + 1/2)\hbar\omega_c]^{1/2}. \tag{2.1.4}$$

The dependence $E_F(B)$ should be taken into account only for small values of N_m ($N_m \le 3$), where the ratio $E/\hbar\omega_c$ is small (see Eq. 2.1.3). The oscillations of the DOS *ρ(E)* with the magnetic field cause corresponding oscillations of all kinetic coefficients. Shubnikov–de Haas (SdH) oscillations are periodical changes of magnetoresistance caused by the changing DOS of the charge carriers on the Fermi level when the intensity of the magnetic field is changed.

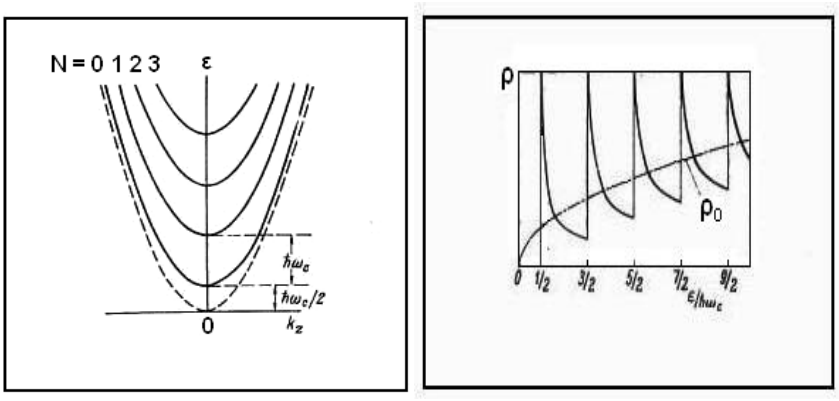

Fig. 2.1.1. Landau energy sub-bands of electrons in the magnetic field $B = B_Z$ (left panel) and the density of electron states *ρ(E)* in the magnetic field (right panel). ρ_0 shows the density of states without magnetic field.

Observation of SdH oscillations is possible under the following conditions:

$$\omega_c \tau >> 1, \tag{2.1.5}$$

$$\hbar\omega_c >> k_B T, \tag{2.1.6}$$

$$E_{F_0} > \hbar\omega_c. \tag{2.1.7}$$

Here, τ is the mean relaxation time. Condition (2.1.5) means that the distance between the Landau levels (LL) must be larger than the broadening of each level $\hbar/\tau$ (or $\mu B >> 1$). It follows from (2.1.6) that the distance between the LL must be larger than their thermal broadening at the temperature of the experiment. Condition (2.1.7) shows the highest limit of the magnetic field when the oscillations disappear. For the observation of SdH

oscillations, the degeneration of electron (hole) gas is necessary ($E_{F_0} >> k_B T$, see Eqs. 2.1.7).

The expression for longitudinal conductivity σ_{ZZ} in the case of the SdH oscillations if charge carriers dissipate on the acoustical phonons [43] at $\boldsymbol{B}$ (0,0, B_Z), $\boldsymbol{j}$ (0,0, j_Z) is written as

$$\frac{\sigma_{zz}}{\sigma_0} = 1 - x\left(\frac{\hbar\omega_c}{2E_F}\right)^{1/2} \sum_{M=1}^{\infty} \frac{(-1)^M M^{1/2}}{sh(Mx)} \exp\left(-\frac{2\pi M}{\omega_c \tau'}\right) \cos\left(\frac{2\pi M E_F}{\hbar\omega_c} - \frac{\pi}{4}\right), \quad (2.1.8)$$

where $x = 2\pi^2 k_B T / \hbar\omega_c$; τ' is the relaxation time, which characterizes the non-thermal broadening of the LL, M is an integer and sh is hyperbolic sinus. The non-thermal broadening of the LL can be caused by some non-homogeneity of the investigated samples and by the dispersion of charge carriers on the defects of the crystal lattice. In some cases, instead of relaxation time, it is convenient to use the effective temperature $T_D = \hbar / \pi k_B \tau'$, known as the Dingle temperature.

Calculation of transversal conductivity $\sigma_{XX} = \sigma_{cl} + \sigma_1 + \sigma_2$ was carried out in [43], where $\sigma_{cl} = e^2 n / m\tau\omega_c^2$ is conductivity in the limit of a classical magnetic field. The expressions in the case of dispersion on the acoustical phonons for the finite temperature, taking into account the broadening levels, are written as

$$\frac{\sigma_1}{\sigma_{cl}} = \frac{5x}{\sqrt{2}}\left(\frac{\hbar\omega_c}{E_F}\right)^{1/2} \sum_{M=1}^{\infty} \frac{(-1)^M M^{1/2}}{sh(Mx)} \exp\left(-\frac{2\pi M}{\omega_c \tau'}\right) \cos\left(\frac{2\pi M E_F}{\hbar\omega_c} - \frac{\pi}{4}\right), \quad (2.1.9)$$

$$\frac{\sigma_2}{\sigma_{cl}} = \frac{3\pi x}{8}\left(\frac{\hbar\omega_c}{E_F}\right) \sum_{M=1}^{\infty} \frac{(-1)^M M}{sh(Mx)} \exp\left(-\frac{2\pi M}{\omega_c \tau'}\right) \cos\left(\frac{2\pi M E_F}{\hbar\omega_c} - \frac{\pi}{2}\right). \quad (2.1.10)$$

The oscillations of the Hall coefficient R_H are theoretically described by the dependence of ρ_{XY} on σ_{XX}. The amplitudes of R_H oscillations should be small, because in theory, they appear only in the second order of (?) dispersion. As it is shown in [43], the period of SdH oscillations P_{SdH} is inversely proportional to S_m:

$$P_{SdH} = \frac{2\pi e}{\hbar S_m} = \frac{2e}{\hbar} \cdot \frac{1}{(3\pi^2 n)^{2/3}}. \quad (2.1.11)$$

Here $S_m = \pi \cdot (3\pi^2 n)^{2/3}$ is the extremal Fermi surface cross-section of the plane perpendicular to the direction of the magnetic field for OR: according to (?) the isotropic quadratic dispersion law. The topology of the Fermi surface of charge carriers can be investigated by studying the anisotropy of the period of the SdH oscillations. In such a

configuration, the period of the SdH oscillations depends only on the concentration of the charge carriers n.

For anisotropic quadratic dispersion, Eq. 2.1.11 may be converted to

$$P_{SdH} = \frac{e\hbar}{cm_c E_F}, \tag{2.1.12}$$

where m_c is the cyclotron mass of charge carriers.

The dependence of P_{SdH} vs. orientation of the Fermi surface in the magnetic field may be presented as follows [43]

$$P_{SdH} = \frac{2\pi e}{h}\left(\frac{N}{3\pi^2 p_{Hall}}\right)^{2/3}\left(m_1 m_2 m_3\right)^{1/3}\left(\frac{\alpha_1^{\,2}}{m_2 m_3}+\frac{\alpha_2^{\,2}}{m_1 m_3}+\frac{\alpha_3^{\,2}}{m_1 m_2}\right)^{1/2}, \tag{2.1.13}$$

where m_i are the main components of the tensor of the effective mass, α_i are the direction cosines of the magnetic field vector, p_{Hall} is the concentration of holes estimated by the Hall effect, and N is the number of equivalent ellipsoids.

The periods of SdH oscillations, corresponding to the extremal crosses of the ellipsoid in the case of ellipsoidal Fermi surfaces of the carriers, are

$$P_{SdH1} = F\left(\frac{m_1^{\,2}}{m_2 m_3}\right)^{1/6};\ P_{SdH2} = F\left(\frac{m_2^{\,2}}{m_1 m_3}\right)^{1/6};\ P_{SdH3} = F\left(\frac{m_3^{\,2}}{m_2 m_1}\right)^{1/6}; \tag{2.1.14}$$

where $F = \frac{2\pi e}{hc}\left(\frac{N}{3\pi^2 p_{Hall}}\right)^{2/3}$. After transformation, we obtain

$$K_1 = \frac{P_{SdH1}^{\,4}\cdot P_{SdH3}^{\,2}}{F^6};\quad K_2 = \left(\frac{P_{SdH2}}{P_{SdH3}}\right)^2;\qquad K_3 = \frac{F^6}{P_{SdH1}\cdot P_{SdH2}}\cdot, \tag{2.1.15}$$

where K_i is the coefficient of anisotropy.

Transformation of Eq. 2.1.13 for the case of magnetic field rotation in (100), (010) or (001) gives

$$P^2{}_{SdH} = a + b\cdot\cos^2\Theta. \tag{2.1.16}$$

The concentration of electrons participating in the SdH effect n_{SdH} may be determined as

$$n_{SdH} = \left(\frac{2\pi e}{hc}\right)^{3/2}\frac{N}{3\pi^2}\left(P_{SdH1}\cdot P_{SdH2}\cdot P_{SdH3}\right)^{-1/2}, \tag{2.1.17}$$

where P_{SdHi} are the periods of the SdH oscillations corresponding to the extremal crosses of the ellipsoidal Fermi surface. The g-factor of free carriers can be found from the spin split of maxima or by using the equation for zero plus maximum, which is given in [43]

$$B_{0^+} = \frac{\hbar}{e}\cdot\left[\frac{4\pi^2 n^2}{|g|}\cdot\frac{m_0}{m_c}\right]^{1/3}. \tag{2.1.18}$$

The estimation of the cyclotron mass of the charge carries, which take part in the SdH oscillations, is performed applying Eq. 2.1.19 from the temperature dependence of the amplitude of the SdH oscillations with an assumption of T_D being independent of temperature [43].

The term for the amplitude ratio of the SdH oscillations at two temperatures T_1 and T_2 corresponds to the transcendental equation

$$\frac{A_{T_1}}{A_{T_2}} = \frac{x_1 / sh \cdot x_1}{x_2 / sh \cdot x_2}, \tag{2.1.19}$$

where A_{T_i} are the amplitudes of SdH oscillations at the temperature T_i and

$$x_i = \frac{2\pi^2 k_B}{\hbar e} \frac{m_c}{m_0} \cdot \frac{T_i}{B_i}. \tag{2.1.20}$$

Solving Eq. 2.1.19 gives the cyclotron mass of the charge carriers, which take part in the SdH oscillations. The amplitude of SdH oscillations is described by

$$A \approx \frac{x \cdot \exp(-2\pi^2 k_B T_D / \cdot \hbar\omega_c)}{(BE_F)^{1/2} \cdot sh(x)}. \tag{2.1.21}$$

Therefore, it is possible to find the Dingle temperature T_D from the inclination of the $\ln\left[A(BE_F)^{1/2} sh(x)/x\right]$ dependence on *1/B*. The comparison of the Dingle temperature value calculated from Hall mobility

$$T_{D\mu} = \frac{\hbar e}{\pi k_B m_c \mu}, \tag{2.1.22}$$

shows whether the dispersion is a dominant reason in the broadening of the Landau levels or not.

Finally, it is possible to make a conclusion that the experimental investigation of the SdH effect is an efficient method for the analysis of the energy band structure of semiconductors. This method allows to study the topology of the Fermi surface in a material and to estimate such important parameters of the energy band structure as the tensor components of the effective mass, *g*-factor, the effective mass of the DOS and, moreover, to evaluate the perfection degree of the grown crystal.

2.2 Hopping conductivity and the Hall effect in presence of several groups of carriers

As shown in the literature, dependences of ln ρ vs. T^{-1} may exhibit several parts of different behavior including consequent intervals of activation and hopping conductivity. Activation conductivity is described by the equation ln $\rho(T)$ = ln $\rho_0 + E_A/(kT)$, when the conductivity is determined mainly by the activation of carriers. For example, holes may be activated from shallow acceptor states to the valence band with the activation energy E_A. However, when neglecting the temperature dependence of the prefactor ρ_0, only approximate values of E_A can be found due to the temperature dependence of the hole mobility.

The hopping conductivity requires a deeper analysis, because in doped crystalline semiconductors, it can be realized via different mechanisms given by a universal equation

$$\rho(T) = D\,T^{m} \exp\left[(T_0/T)^{p}\right] \qquad (2.2.1)$$

where D is a constant, $m = p$ for the hydrogenic wave functions of the localized electrons and T_0 is a characteristic temperature [54]. The case of $p = 1$ corresponds to the regime of nearest-neighbor hopping (NNH) conductivity and $p = 1/4$ and $p = 1/2$ to the Mott [55] and the Shklovsky–Efros (SE) [54] types of variable-range hopping (VRH) conductivity, respectively. The SE-VRH conductivity sets in when the Coulomb interaction between the charge carriers becomes important leading to the formation of a Coulomb gap, Δ, around the Fermi level, μ, in the density of localized states (DOS). The Mott VRH conductivity is observed when the Coulomb interaction can be neglected, but the disorder is high enough to make the tunneling of the electrons between the nearest sites energetically unfavorable [54, 55]. The characteristic temperature in the case of $p = 1$ is usually $T_0 = E_{NNH} / k$, where E_{NNH} is the activation energy of the nearest-neighbor hopping (NNH) conductivity. For the Mott- and SE-VRH conductivity mechanisms T_0 in Eq. (2.2.1) is replaced by

$$T_{0M} = \beta_M / [\,k\,g(\mu)\,a^3], \qquad T_{0SE} = \beta_{SE} e^2 / (k\,\kappa\,a), \qquad (2.2.2)$$

respectively, where $g(\mu)$ is the DOS at the Fermi level, κ is the dielectric permittivity, $\beta_M = 21$, $\beta_{SE} = 2.8$ and $a = (a_1 a_2 a_3)^{1/3}$ is the mean localization radius [54]. In this case a_i (i = 1, 2 and 3) scales the exponential decay of the anisotropic impurity wave functions of p-CdSb in the ith direction. The anisotropy of a_i in this case is connected to that of m_i as follows: for $N_A << N_C$, what is far from metal – insulator transition (MIT) $a_i = a_{0i} \equiv \hbar\,(2\,m_i$

$E_A)^{-1/2}$ and for $N_A \to N_C$ (close to MIT) $a_i = a_{0i} (1 - N_A / N_C)^{\nu}$. Here, N_A and N_C are the acceptor concentration and the critical concentration of MIT, respectively, and ν is the critical exponent of the correlation length [54–56]. We may also introduce the mean parameter $a_0 \equiv (a_{01}a_{02}a_{03})^{1/3}$ to obtain a general expression

$$a = a_0 (1 - N_A / N_C)^{\nu}, \tag{2.2.3}$$

which is the same as in an isotropic material [56]. To find the regime of the hopping conductivity at $B = 0$, it is convenient to rewrite Eq. (2.2.1) as

$$\ln [E_a /(kT) + m] = \ln p + p \ln T_0 + p \ln (1/T), \tag{2.2.4}$$

where $E_a \equiv d\ ln\ \rho\ /\ d\ (kT)^{-1}$ is the local activation energy [54], so that for a certain conductivity mechanism, the left-hand side of Eq. (2.2.4) would be a linear function of ln $(1/T)$ and p would be given by the slope of the plot ln $[E_a /(kT) + m]$ vs. ln $(1/T)$. For SE NNH conductivity Eq. (2.2.1) may be transferred to the expression

$$\rho (T) = \rho_0 (T) \exp (\varepsilon / kT), \tag{2.2.5}$$

where the activation energy ε is independent of the temperature and the prefactor $\rho_0 (T) \sim T$ [54]. Far from the MIT, the value of ε does not depend on B, while the dependence of ρ_0 on B is different in the intervals of weak ($B < B_c$) and strong ($B > B_c$) magnetic fields.

Theory [54] predicts

$$\ln \frac{\rho_0 (B)}{\rho_0 (0)} = CB^2 \text{ (for } B < B_c) \tag{2.2.6}$$

and $$\ln [\rho (T, B) / \rho_0] = \chi (B) (B / T)^{1/3} \text{ (for } B > B_c), \tag{2.2.7}$$

Here $C = t\ e^2\ a\ /\ (\hbar^2 N_i)$, $\chi (B) = \chi_0 [g (E_F)\ \xi (B)]^{-1/3}$, $\chi_0 = [2.1e/(\hbar k_B)]^{1/3}$, where ξ is the localization radius scaling the exponential decay of the wave function of a localized electron, $g (E_F)$ is the DOS at the Fermi level, a is the localization radius of the charge carriers determining the space decay of the impurity wave function, N_i is the concentration of the impurities involved in the hopping charge transfer and $t = 0.036$ [54]. In addition to the shrinking of the wave functions, application of a strong magnetic field increases the energy of the impurity level, E, which in the case of $B_0 < B < 100\ B_0$ obeys the law $E (B) \approx b\ B^{1/3}$, where $B_0 = \hbar / (ea^2)$ is the field at which the magnetic length becomes equal to the localization radius and b is a constant.

In the vicinity to the MIT, the localization radius depends on N according to the scaling law $a\,(N_i) = a_0\,(1 - N_i / N_c)^{-\nu}$, where N_c is the critical concentration corresponding to the MIT and $\nu \approx 1$ is the critical exponent [55, 56].

The crossover of the weak and the strong fields can be estimated with the equations

$$B_c = \hbar N^{1/3} / (ea), \tag{2.2.8}$$

where a is the localization radius in zero field or, after modification

$$B_c \approx \frac{\hbar}{e}\frac{[g(E_F)k_BT]^{1/4}}{\xi^{5/4}}. \tag{2.2.9}$$

The expressions above are valid for semiconductors with isotropic impurity wave functions. If a wave function is anisotropic, magnetoresistance (MR) can depend on the orientation of $\boldsymbol{B}$ with respect to the crystallographic axes. This dependence stems from different values of the carrier effective mass in the directions perpendicular to the magnetic field, leading to the different elasticity of the wave function to the magnetic shrinkage. On the other hand, the right-hand sides of Eqs. (2.2.8) and (2.2.9) are insensitive in an anisotropic semiconductor to the direction of $\boldsymbol{j}$ with respect to the crystallographic axes [54].

In p-CdSb, the anisotropy of the MR in the magnetic field can be found in an almost similar way as proposed in [54] for n-Ge subjected to strong compression along the [111] direction. By a transition of the coordinate system using $a^* = (a_1\ a_2\ a_3)^{1/3}$ as the mean localization radius, the Hamiltonian of the carrier with an anisotropic effective mass in the magnetic field can be reduced to a form of a carrier with an isotropic mass $m^* = (m_1\ m_2\ m_3)^{1/3}$.

Finally, the magnetic field dependence of the resistivity in p-CdSb can be conveniently expressed for $B < B_c$ as

$$\ln\left[\frac{\rho_0(B)}{\rho_0(0)}\right]_{ij} = C_{ij}B^2 \tag{2.2.10}$$

and for $B > B_c$

$$\ln\left[\frac{\rho_0(B)}{\rho_0^{/}}\right]_{ij} = S_{ij}B^{7/12} \tag{2.2.11}$$

where

$$C_{ij} = t\frac{e^2 a_0^*}{\hbar^2 N_i (1 - N_i / N_c)^{\nu}} p_j^2 \tag{2.2.12}$$

and $$S_{ij} = q\left[\frac{e(1-N_i/N_c)^{\nu}}{\alpha\hbar N_i}\right]^{1/2} p_j^{7/12}. \qquad (2.2.13)$$

In Eqs. (2.2.10 - 13), the subscripts i = 1, 2, 3 and j = 1, 2, 3 refer to the direction of electrical current (along the ith crystallographic axis) and to the direction of $\boldsymbol{B}$ (along the jth crystallographic axis), respectively.

The models of different mechanisms of hopping conductivity reviewed above and the corresponding formulas will be used in Chapter 3 for the description of the behavior of p- and n-CdSb at low temperatures in a magnetic field.

The decrease of the Hall coefficient, R_H (B), in low magnetic fields down to a minimum with increasing field suggests a contribution of different groups of charge carriers, one of which can be associated with the high-mobility electrons of conduction band (CB) [Publication 2, 77]. However, close to liquid helium temperatures, these electrons may participate in the SdH effect providing an oscillating contribution to R_H (B) [Publication 2, 77]. Therefore, our analysis of the Hall effect in the low-field interval of B up to the minimum of R_H (B) using the two-band model [59] should be limited to conditions of small oscillatory contribution to R_H (B) or when the magnetic quantization of CB can be neglected. The Hall effect is treated classically, restricting the analysis only to the itinerant carriers and taking the Hall factor equal to unity.

Under these conditions, the expression of the Hall coefficient

$$R_H = \frac{n_1\mu_1^2 + n_2\mu_2^2 + (n_1+n_2)\mu_1^2\mu_2^2B^2}{e(n_1\mu_1 + n_2\mu_2)^2 + e(n_1+n_2)^2\mu_1^2\mu_2^2B^2}, \qquad (2.2.14)$$

in the two-band model in the low-field interval contains the concentrations n_1, n_2 and the mobilities μ_1, μ_2 of the high- and low-mobility electrons, respectively. All these parameters are independent of B, whereas the violation of their constancy in the field exceeding that of the minimum of R_H (B) is connected to the onset of the high-field limit and will be analyzed separately. To simplify the analysis, we may use the expression of Eq. (2.2.14) in the form [60, 61]

$$R_H = \frac{R_0 + R_\infty\mu^2B^2}{1+\mu^2B^2}, \qquad (2.2.15)$$

where only two adjustable parameters, μ and R_∞ (the Hall coefficient in the infinite magnetic field), exist because R_0 (the Hall coefficient in zero magnetic field) can be found with a small error directly from experiment at the lowest fields of $B \approx 0.2 - 0.3$ T. Finally, by solving a system of equations containing the expressions of R_0, R_∞, μ and $\rho^{-1} = e\,(n_1\mu_1 + n_2\,\mu_2)$, where ρ is the zero-field resistivity, we obtain the unknown parameters μ_j and n_j (j = 1, 2) (see [P5]).

Using experimental values of R_0, R_∞ and μ obtained from the best fit of R (B) with Eq. (2.2.15), the functions n_j (T) and μ_j (T) (j = 1, 2) can also be evaluated (see [Publication 5]).

The analysis of μ_1 (T) is made with the equation

$$\frac{1}{\mu} = \frac{1}{\mu_{ac,ii}} + \frac{1}{\mu_{ni}} \tag{2.2.16}$$

where $\mu_{ac,ii} = \mu_{ac}\, G\, [6(\mu_{ac}/\mu_{ii})^{1/2}]$ is the contribution resulting from the combined acoustic phonon (μ_{ac}) and ionized impurity (μ_{ii}) scattering and μ_{ni} is the contribution to the neutral impurity scattering [65].

2.3 Sample preparation and experimental procedure

Intentionally undoped single crystals of Cadmium Antimonide and doped with Ag and In on the level of 0.01–0.1 weight % were grown using horizontal zone melting technique [16]. The growth direction of the ingot, as set by the orientation of the seed crystal, was along the [001] axis, because in CdSb, there exist two chip planes, perpendicular to [100] and [010] directions. In all cases, the synthesis of the polycrystalline material was performed from elementary Cd and Sb, where the uncontrolled impurity content was less than 10^{-5}. The synthesized material was later used for growing doped and undoped crystals. The obtained single crystals were oriented in n X-ray diffractometer.

The samples with the size 1x1.5x5.5 mm^3 and the special rectangular shape for the transport measurements were cut out from the CdSb ingots along the three main crystallographic axes and abraded with abrading powders. The contacts were soldered by the Bi-Sn alloy with a low melting temperature, and contact wires were bound in pairs to decrease the influence of the magnetic field sweeping on the measuring circuit.

The measurements of the transport properties of CdSb were performed in a steady magnetic field up to 12 T and in a pulsed magnetic field up to 30 T in the temperature range of 1.6–300 K. In the case of the steady magnetic field, the magnetic field was measured by a calibrated Hall probe located close to the sample. The temperature of the experiment in the temperature range of 4.2–300 K was stabilized on the required level by a temperature controller and it was measured by Cu–Cu:Fe thermocouple, which had a good thermal contact with the sample. The experiments in the temperature range 1.6–4.2 K were performed when pumping liquid helium, and the temperature was controlled by a mercury McLeod manometer measuring the pressure of helium vapors above the liquid

helium surface. The pressure of liquid helium vapors and the corresponding temperature was stabilized on the required level by the membrane monostate.

The speed of magnetic field sweeping was not more than 0.3 T/min. The signals from the sample were recorded for opposite magnetic field polarities and also for increasing and decreasing of the magnetic field to exclude self-inductance voltage in the measuring circuits in spite of the bind in pairs contact wires. Measuring of the signals is carried out with digital voltmeters with an input impedance more than 1 GΩ connected with a computer via a data acquisition card. The recorded data are processed by a LabView-based computer program and are in a ready form for plotting by a graphical program. Highly stabilized programmable power supplies were used for electric currents of the sample and the Hall probe.

Rotation of the sample in a magnetic field was carried out by a specially prepared sample holder, which allows rotating the sample for 110^{o} around the horizontal axis. The samples were rotated not only from the transverse orientation to the longitudinal one, but also in pure transverse position. In this case, the Hall contacts of the sample were shortcut to exclude the contribution to magnetoresistance from the Hall voltage, which depends on the angle. Rotation of the samples was performed mainly in one of three perpendicular planes (100), (010) or (001). For checking the assumption [38, 39] of the location of the energy band extrema in other planes, the magnetic field was rotated also from the [101] direction to [010] and from the [110] direction to [001].

The investigations of the transport properties were performed also in a pulse magnetic field (PMF) up to 30 T. Such a high field can be obtained as a short pulse of a magnetic field inside the specially prepared coil (solenoid), through which a battery of capacitors is discharged. Because the connection of the inductance coil and the capacitor is an oscillatory contour, an electrical current in such a circuit (and the magnetic field in the coil) will follow the cosine law vs. duration of the pulse. The solenoid is cooled by liquid nitrogen. The pulse length was 8 ms, and the signal from different pairs of the potential contacts was recorded with a step of 1 μs.

The amplitude of the created field was measured by the calibrated measuring coil located close to the sample and connected to the data acquisition computer card with a computer. Knowledge of the square of the coil, duration of the pulse and the signal from the coil allows calculating the amplitude of magnetic field. The error in the magnetic field strength was not higher than 0.2 %. The temperature of the sample during the PMF measurements was measured, regulated and stabilized in the same way as in the superconducting solenoid.

The analyzes of the obtained results were performed using formulas applicable for the isothermal conditions of the experiment. The experimental conditions can be considered isothermal with good accuracy, because the temperature gradients along or across the samples were very small. Overheating of the samples was checked by estimating an electric current limit value that is equal to the current value at which non-linear IV characteristic begins. In all the experiments, the applied value of electric current was at least twice smaller than the limit value. The contacts on the samples were placed in accordance with the standard six-probe-scheme.

The kinetic coefficients were calculated using the experimental results by the standard formulas:

the Hall coefficient $R_{Hall} = \frac{V_{Hall} \cdot d}{I_x B_z}$, (2.3.1)

where V_{Hall} is the Hall voltage, d is the dimension of the sample along the magnetic field, I_x is the electric current through the sample and B_z is the magnetic field component perpendicular to the plane of the potential contacts.

Specific electrical conductivity $\sigma = \frac{I \cdot l}{V_\sigma S}$, (2.3.2)

where I is the electric current, l is the distance between contacts, V_σ is the potential difference between contacts and S is the square of the cross-section of the sample perpendicular to the electric current.

3 Results

This Chapter presents the results of the investigation of the transport phenomena in the undoped Cadmium Antimonide and doped by shallow impurities. The Shubnikov–de Haas (SdH) oscillations in CdSb were detected for the first time in this work. Therefore, the topology of the Fermi surfaces of holes and electrons in this material was defined, the energy band parameters were estimated, and a model for the energy band structure was proposed and compared with those proposed in the literature. The study of the transport phenomena in CdSb in high magnetic fields in a wide temperature range opened new opportunities to understand the energy spectrum of electrons and holes near the edges of conductivity and valence energy bands, and to determine the types of mechanisms of hopping conductivity in this material. This became possible because of the estimation of the energy band parameters when studying the SdH effect in this material.

3.1 Quantum transport phenomena in p-CdSb and its energy band structure

3.1.1 Fermi surface of holes in Cadmium Antimonide

The anisotropy of p-CdSb was observed already during the first studies. The extensive experimental and theoretical studies on the energy band structure of CdSb, presented in Chapter 1.2, yield a wide spectrum of the possible energy band parameters. These results differ considerably also on the principle level. That is why the energy band structure of this semiconductor was a question of special interest. The detection of the SdH oscillations gave for the first time a straightforward opportunity to define which model of the energy band structure is correct. Because of the anisotropy, it is obvious that the SdH effect in p-CdSb should be studied with different orientations of the magnetic field relative to the crystal lattice of the sample.

The detection of the SdH oscillations stimulated new interest in the CdSb, and in [51], investigations were continued on the SdH effect in CdSb in a wide temperature range. Further, in [51, 82–86], studies for the cyclotron resonance and lattice excitations in p-CdSb were performed in a wide range of temperatures and illumination energies. All the results connected to the quantum effects in CdSb are compared below. The p-CdSb samples doped with different Ag concentrations were measured with all possible types of sample configurations. The long edge of sample (i.e., electric current $\boldsymbol{j}$) was parallel to the $\boldsymbol{a}$ [**100**], $\boldsymbol{b}$ [**010**] and $\boldsymbol{c}$ [**001**] axes, respectively. The direction of the magnetic field $\boldsymbol{B}$ in the

transversal configuration was parallel to ***a***, ***b***; and ***c*** given in the last digit 1, 2, 3 in the sample number, respectively.

*Table 3.1.1. Hall concentration, p_{Hall}, the Hall mobility, μ_{Hall}, specific conductivity, σ, periods of SdH oscillations with magnetic field parallel to the corresponding crystal axes, P_{SdHi} , number of equivalent valence band extrema, N, orientation of electric current, **j**, and magnetic field **B**, in the investigated p-CdSb samples at 4.2 K*

Sample number (SN)	p_{Hall}, 10^{17} cm^{-3}	σ, Ω^{-1} cm^{-1}	μ_{Hall}, $cm^2/V\ s$	P_{SdH1}, 10^{-2} T^{-1}	P_{SdH2}, 10^{-2} T^{-1}	P_{SdH3}, 10^{-2} T^{-1}	$N = \frac{p_{Hall}}{p_{SdH}}$	***j***/ ***B***
36b1	1.85	16.4	553	15.00	22.5	-		[010]/ [100]
36b3	1.90	16.6	546	14.95	-	10.77	2.17	[010]/ [001]
36c2	1.80	42.6	1480	7.10	22.5	10.82		[001]/ [010]
51b1	6.10	65.9	675	7.06	11.2	-		[010]/ [100]
51c1	5.90	182.2	1930	-	-	5.18	2.2	[001]/ [100]
51b2	6.10	63.4	650	1.90	11.2	5.20		[010]/ [010]
27b1	46.0	305	410	1.80	2.80	-		[010]/ [100]
27c1	45.0	980	1360	-	-	1.32	2.1	[001]/ [100]
27b2	45.6	246	340	1.3	2.78	1.37		[010]/ [010]
D1b1	96.6	702	454	1.29	1.8	-		[010]/ [100]
D1c2	96.8	-	-	-	1.78	-	2.3	[001]/ [010]
D1a1	96.2	-	-	-	1.76	-		[100]/
D1a2	96.7	-	-	-	-	0.9		[100]/ [010]

The measurements of all specimens were made in accordance with the procedure described in Chapter 2.3. The parameters of the investigated samples, their crystal orientation and orientation in the magnetic field are presented in Table 3.1.1.

The SdH oscillations in some of the investigated samples are presented in Figs. 3.1.1–3.1.2. It can be seen that the SdH oscillations are moving in the magnetic field when the crystal is rotating. This gives evidence of the anisotropy of the Fermi surface of holes in CdSb (see Chapter 2.1). Only one period of the SdH oscillations was observed in each curve in all the investigated samples showing existence of only one group of holes participating in the SdH effect.

The angle dependences of the period of the SdH oscillations are presented in Fig. 3.1.3 for the three investigated samples. Good correlation is observed between the dots (experimental data) and the solid lines (calculations by Eq. 2.1.11 of P_{SdH} changes with the angle under the assumption of the ellipsoidal shape of the Fermi surface of holes), when the samples were rotated between the crystallographic axes 1–3.

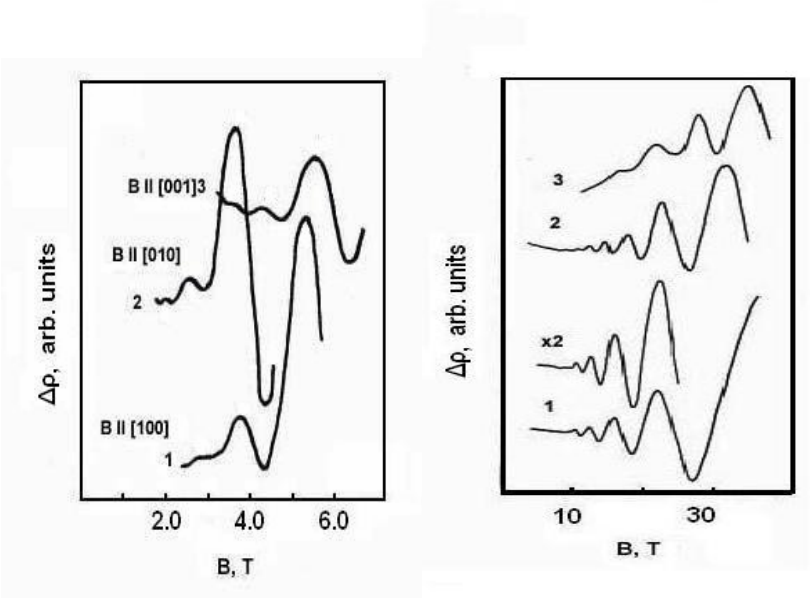

Fig. 3.1.1**.** SdH oscillations in the p-CdSb samples 51 (left panel) and D1 (right panel) at T = 1.6 K with a magnetic field along the main axes of the crystal. The curves 1, 2, 3 are for $\boldsymbol{B}$ || **[100]**, for $\boldsymbol{B}$ || **[010]** and for $\boldsymbol{B}$ || **[001],** respectively [Publication 1].

If the Fermi surface of holes is close to elliptical, the experimental points of P^2_{SdH} vs. $cos^2\theta$, where θ is the angle between the magnetic field and the corresponding crystal axes, should follow the straight line in accordance with Eq. (2.1.16). Such a dependence for one of the samples is presented in Fig. 3.1.4.

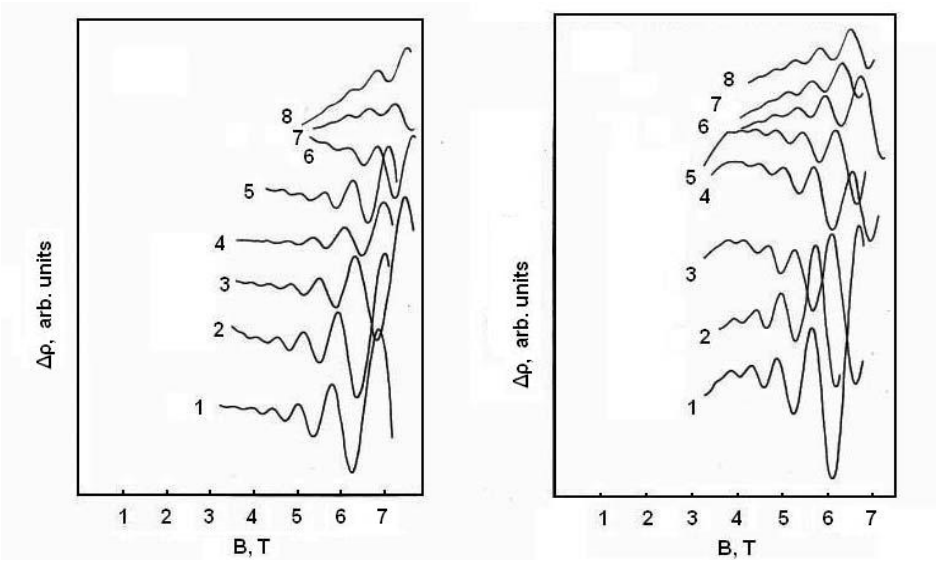

Fig. 3.1.2**.** Field dependences of the SdH oscillations of the p-CdSb sample 27 at T = 1.6 K when turning the magnetic field from ***B*** || **[010]** (curve 1) to ***B*** || **[001]** (curve 8) (left panel) and when turning the magnetic field from ***B*** || **[010]** (curve 1) to ***B*** || **[100]** (curve 8) (right panel) with the step 12°51'.

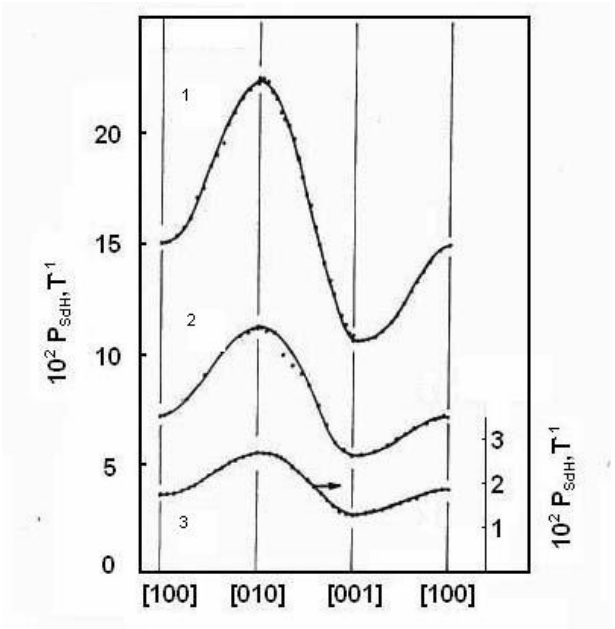

Fig. 3.1.3**.** Angle dependences of the SdH periods in p-CdSb when rotating the magnetic field in the planes (100), (010) and (001). The curves 1, 2 and 3 belong to the samples 36, 51 and 27, respectively. The dots are experimental data and the lines represent the

calculations of the angle dependences in the ellipsoidal approximation of the Fermi surfaces of holes [Publication 1].

From the slope b and cut-off a, it is possible to estimate the coefficients of the anisotropy of the effective mass of holes K_i : $K_1 = m_1/m_2$; $K_2 = m_2/m_3$; $K_3 = m_3/m_1$, because the comparison of Eqs. (2.1.15) shows that, for example, $K_2 = (a+b)/a$, where $a = A/m_1m_2$ and $b = (K_2 - 1)(A/m_1m_2)$. A similar procedure for other rotations allows the calculation of all anisotropy coefficients of the effective masses of holes, presented in Table 3.1.2. All the anisotropy coefficients of the effective masses of holes in CdSb, calculated from Eq. (2.1.16) and presented in Table 3.1.2, are in a good agreement with those calculated from the experimental components of the effective mass tensor shown below in Chapter 3.1.2.

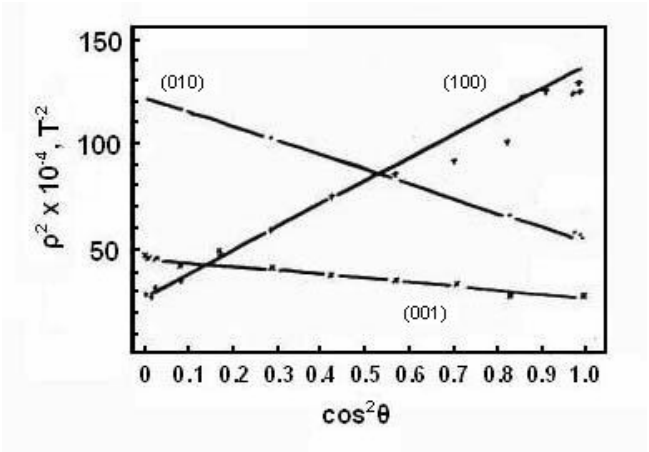

Fig. 3.1.4. Dependences of the square of the period of the SdH oscillations, P^2_{SdHi} ,on $\cos^2\Theta$ in p-CdSb, where Θ is the angle of the orientation of the magnetic field relative to the crystal axes in the planes (100), (010) and (001) for the sample 51. The lines are linear fits to Eq. 2.1.16.

Hence, it is shown by the experiments (see Fig. 3.1.3) that the Fermi surface of holes in CdSb is close to an ellipsoid of general form with the main axes parallel to the crystallographic directions [100], [010] and [001].

However, to choose the right model of the energy band structure, it does not suffice to know the parameters of the Fermi surface, but it is also important to know the number of the equivalent extrema in the Brillouin zone.

Table 3.1.2. Coefficients of the anisotropy K_i of the effective masses of holes in CdSb estimated by different methods

SN	From $P_{SdH}^{\ 2} = a + b \cdot \cos^2 \Theta$			From the extremal values of P_{SdHi}			From the components of the effective masses tensor		
	K_1	K_2	K_3	K_1	K_2	K_3	K_1	K_2	K_3
36	0.50	3.90	0.49	0.42	4.34	0.55	0.47	4.70	0.45
51	0.51	4.40	0.41	0.58	4.64	0.37	0.41	5.10	0.48
27	0.41	4.38	0.48	0.44	4.44	0.51	0.53	3.62	0.52
D1	-	-	-	-	4.0	-	0.58	3.46	0.52

The number of equivalent ellipsoids may be determined from the ratio of the Hall concentration of the carriers p_{Hall} and the concentration of the carriers participating in the SdH effect p_{SdH}. The value of $N = p_{Hall}/p_{SdH}$ is very close to 2 for all the investigated samples (see Table 3.1.1), in other words, the Fermi surface of holes in CdSb consists of two equivalent ellipsoids.

The model of the energy band structure of CdSb, in which there are two equivalent maxima of the valence band located on the axis [100] in the *k*-space point (0.8 π/a; 0; 0), was first proposed in [38], where the theoretical calculations of the energy band structure were performed by the pseudo potential method.

Thus, based on the obtained experimental results and calculations performed, it is possible to conclude that the Fermi surface of holes in CdSb consists of two ellipsoids of general form, and the phenomena taking in CdSb, may be described with the theoretical calculations presented in [38, 39, 82–87].

3.1.2 Energy band parameters of p-CdSb

Building a model for energy band structure requires knowledge about the number of equivalent extrema of the energy bands N, the components of the effective mass tensor m_i and the effective mass of the DOS m_p. The number of equivalent extrema of the valence energy band, $N_p = 2$, was estimated in the previous chapter from the ratio of the Hall concentrations of holes versus the concentration of holes participating in the SdH effect.

The components of the effective mass tensor m_i can be calculated if the Fermi surface is elliptical and when the cyclotron effective masses of holes m_{ci} along the main ellipsoid axes are known. The value of the cyclotron mass may be expressed as

$$\frac{1}{m_{ci}^{\,2}} = \frac{\alpha^2{}_1}{m_2 m_3} + \frac{\alpha^2{}_2}{m_1 m_3} + \frac{\alpha^2{}_3}{m_1 m_2}, \tag{3.1.1}$$

where α_i are the direction cosines of the magnetic field vector relative to $\boldsymbol{i}$ = 1, 2, 3 axes. After transformation, we obtain the system of equations

$$m_1 = \frac{m_{c2} m_{c3}}{m_{c1}}, \qquad m_2 = \frac{m_{c1} m_{c3}}{m_{c2}}, \qquad m_3 = \frac{m_{c1} m_{c2}}{m_{c3}}. \tag{3.1.2}$$

The cyclotron effective masses of holes m_{ci} along the corresponding directions of the crystal were estimated from the temperature dependence of the amplitudes of the SdH oscillations applying Eqs. (2.1.19–2.1.20); the results are presented in Table 3.1.3. The effective mass of the DOS, m_p, in CdSb for the investigated samples was estimated with Eq. (3.1.3) and is presented in Table 3.1.3.

$$m_p = N^{2/3}\left(m_1 m_2 m_3\right)^{1/3} \tag{3.1.3}$$

The data in Table 3.1.3 show that m_{ci} depends on the concentration of carriers in the valence band of CdSb, i.e., the valence band in this material is not exactly parabolic. In all later publications on quantum effects in CdSb [51, 82–86], an acceptable agreement between the SdH data and results obtained in cyclotron resonance (CR) studies was noticed (see Table 3.1.3) in spite of the fact that the Fermi energy level was quite different in the CR cases.

However, it is necessary to emphasize that the cyclotron resonance provides the most direct spectroscopy and gives a refinement of the parameters. It was found in [82] that the values of the cyclotron masses of holes determined in [51] are not completely correct (see Table 3.1.3).

A peculiar behavior noted in [82] takes place in CdSb: at low levels of the Fermi energy, the cyclotron masses decrease when increasing the excitation energy. It can also be seen in Table 3.1.3 that the dependence of the cyclotron mass vs. the Fermi energy level is not monotonic: when the Hall concentration of holes is small, it follows the peculiarity, noticed in [82], then, it has minima at $E_F \approx 10$ meV and starts to grow in the heavy degenerate case.

Detailed analyzes were made in [83, 84] for the LLs in CdSb for the arbitrary directions of the magnetic field. It was stated in [84] that the cyclotron masses at energies higher that 10 meV calculated with the new set of parameters agree with the SdH data. It

was stated OR assumed in [86] that the momentum effective masses in CdSb must not be directly derived from a simple ellipsoidal model, and their determination requires a more suitable calculation than the one developed in [87].

Such an assumption may be confirmed by the fact that the shape of the Fermi surface in p-CdSb is not an exact ellipsoid for all concentrations of holes. The experimental values of the SdH period of oscillations are different from elliptical at some directions of the magnetic field, as it can be seen in Fig. 3.1.3 and in Fig. 2 in [Publication 1] for the sample 51; we can see that the real volume of the Fermi surface is larger than the corresponding elliptical one. To estimate the exact deviation of the Fermi surface from the elliptical- shaped one, it is necessary to study the angle dependences of the SdH period not only in the main crystal planes but also in the intermediate ones.

Table 3.1.3 Fermi energy, the Hall concentration, p_{Hall}, cyclotron masses, m_{ci}, and the main components of the effective mass tensor of holes, m_i, in CdSb

SN	E_F, *meV*	p_{Hall}, 10^{17} cm^{-3}	m_{ci}/m_0			$\frac{m_1}{m_0}$	$\frac{m_2}{m_0}$	$\frac{m_3}{m_0}$	$\frac{m_p}{m_0}$
			***B* || [100]**	***B* || [010]**	***B* || [001]**				
[82]	-	0.02	0.275± 0.005	0.18±0.005	0.414± 0.01	0.27	0.63	0.12	0.43
36	-	1.9	0.22±0.01	0.15±0.01	-	-	-	-	-
51	6.7	6.0	0.25±0.01	0.16±0.01	0.36±0.01	0.23	0.56	0.11	0.39
41/1	10.4	9.1	0.24±0.01	0.16±0.01	0.34±0.01	0.23	0.50	0.11	0.33
41/2	25.8	15.0	0.27±0.01	0.18±0.01	0.38±0.01	0.25	0.58	0.13	0.42
134	52.2	86.0	0.30±0.01	0.21±0.01	0.42±0.03	0.29	0.6	0.15	0.47
[51]	-	0.02	0.16±0.01	0.12±0.01	0.32±0.01	0.24	0.43	0.06	0.29

A half width, K_{Fi}, of the Fermi surface ellipsoids in *k*-space can be calculated from the general principles of geometry as follows:

$$K_{F1}=\left(\frac{2\pi e}{hc}\cdot\frac{P_{SdH1}}{P_{SdH2}\cdot P_{SdH3}}\right)^{1/2}, K_{F2}=\left(\frac{2\pi e}{hc}\cdot\frac{P_{SdH2}}{P_{SdH1}\cdot P_{SdH3}}\right)^{1/2} K_{F3}=\left(\frac{2\pi e}{hc}\cdot\frac{P_{SdH3}}{P_{SdH1}\cdot P_{SdH2}}\right)^{1/2} \quad (3.1.5)$$

where P_{SdHi} is the period of the SdH oscillation when the magnetic field is along the crystallographic direction *i*, respectively. The half width of the ellipsoid along the corresponding direction for every investigated sample is presented in Table 3.1.4.

*Table 3.1.4. Hall concentration, p_{Hall}, the linear dimensions (half width) of the Fermi surface ellipsoids of holes in k-space, K_{Fi} , and the orientation of **j** in the CdSb samples*

Sample number	p_{Hall}, 10^{17} cm^{-3}	K_{F1} 10^6 cm^{-1}	K_{F2} 10^6 cm^{-1}	K_{F3} 10^6 cm^{-1}	Orientation
36b1	1.85				[010]
36b3	1.90	1.3	2.17	0.96	[010]
36c2	1.80				[001]
51b1	6.10				[010]
51c1	5.90	1.94	3.01	1.40	[001]
51b2	6.10				[010]
27b1	46.0				[010]
27c1	45.0	3.92	5.86	2.73	[001]
27b2	45.6				[010]
D1b1	96.6				[010]
D1c1	96.4				[001]
D1c2	96.8	4.96	6.8	3.44	[001]
D1a1	96.2				[100]
D1a2	96.7				[100]

The cross-section of the first Brillouin zone by plane (001) piloted via Γ point in CdSb is presented in Fig. 3.1.5. The concentric ellipses around points (±0.8 π/a; 0; 0) are the boundaries of the cross-sections of the Fermi surfaces of holes in the investigated samples.

Usually, *g*-factor is estimated from the splitting of SdH maxima with small quantum numbers N_m. The SdH oscillations for the sample 51 are presented in Fig. 3.1.6 (curve 1) for $\boldsymbol{B} \parallel \mathbf{[001]} \perp \boldsymbol{j} \parallel \mathbf{[010]}$. It is clear that the maxima with $N_m > 0$ are not splitted and the influence of a spin is visible only because of the presence of the 0^+ SdH maximum.

After transformation of Eqs. (2.1.11) and (2.1.18), we obtain

$$g_i = \frac{16}{3}\frac{m_0}{m_{ci}}\left(P_{SdHi}\cdot B_{0_i^+}\right)^{-3}, \qquad (3.1.4)$$

where g_i is the *g*-factor and B_{0^+i} is a position of the 0^+ SdH maximum in the magnetic field directed along the corresponding ***i*** direction.

The investigations of the SdH oscillations in pulsed magnetic fields were performed for the investigation of the Fermi surface anisotropy in p-CdSb and the anisotropy of the factor of spectroscopic splitting, *g,* of the LLs in a magnetic field. The quantum oscillations of the Hall coefficient (OHC) also are observed in p-CdSb and are presented in Fig. 3.1.6 for the sample 51.

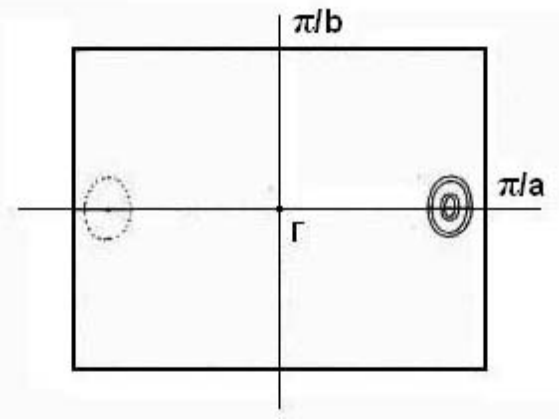

Fig. 3.1.5**.** Section of the first Brillouin zone of CdSb via *Γ*-point by the plane (001). Concentric ellipses around the points (±0.8 π/a; 0) are the borders of the Fermi surfaces of the investigated samples, where the internal one is for the sample 36 and the external one for the sample D1.

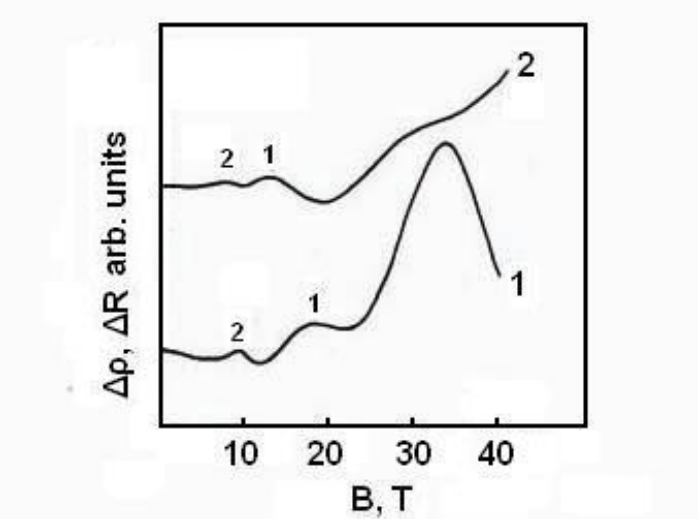

Fig. 3.1.6**.** Oscillating part of the Hall coefficient (curve 1) and SdH quantum oscillations (curve 2) in the p-CdSb sample 51 at T = 1.6 K for ***B*** **|| [001].**

The Hall coefficient R_H may be described as [43]

$$R_{Hall} = \frac{1}{B}\frac{\sigma_{xy}}{\sigma_{xy}^{\ 2} + \sigma_{xx}^{\ 2}}, \qquad (3.1.5)$$

where σ_{xx} and σ_{xy} are the components of the conductivity tensor. The reason of the OHC in the presence of one group of carriers may be the oscillating character of σ_{xx}, as a small term in Eq. (3.1.5).

In this case, the quantum OHC are small and have the same period as the SdH oscillations (σ_{xx}), but are shifted for $\pi/4$ towards strong magnetic fields. This feature opens an opportunity to use the Hall oscillations instead of the SdH ones, because it is more convenient to estimate the position of the 0^+ maximum, which is more clearly visible in the Hall effect than in the SdH effect (see Fig. 3.1.6). This observation is very useful in the cases ***B*** || **[100]** $\perp$ ***j***||**[001]** and ***B*** || **[010]** $\perp$ ***j***||**[001],** where it is impossible to see a 0^+ maximum of the SdH oscillations, but a 0^+ maximum of the Hall effect is easier to detect. The positions of 0^+ maxima of SdH $B_0{}^+{}_{SdH}$ and the Hall effects $B_0{}^+{}_{Hall}$ for different orientations of the CdSb crystal in the magnetic field are presented in Table 3.1.5 together with the *g*-factor values calculated in accordance with Eq. (3.1.5).

Table 3.1.5 Positions of zero-plus maxima of the SdH oscillations in a magnetic field, $B_0{}^+$, and the values of g-factor in p-CdSb

	B || **[100]**	***B*** || **[010]**	***B*** || **[001]**
$B_0{}^+{}_{SdH}$, T	18.3	14.6	27.1
$B_0{}^+{}_{Hall}$, T	22.1	20.5	33.0
g-factor	10 ± 3	7 ± 2	5.3 ± 0.5

Considerable inaccuracy in the *g*-factor value when ***B*** || **[100]** and ***B*** || **[010]** is caused by the overlapping of the 1st maximum of the Hall oscillations and the 0^+ one leading to an error in the estimation of $B_0{}^+{}_{Hall}$.

3.1.3 Hopping conductivity and energy spectrum near the valence band edge in CdSb

The investigations of the types of conductivity of p-CdSb by the experimental methods described in Chapter 2.3 and analyses of the obtained results became possible only because of the estimation of the CdSb valence band parameters during the investigations

of the SdH effect in p-CdSb (see Chapters 3.1.1, 3.1.2, [Publication 1]). The SdH measurements in the heavily doped p-CdSb give the effective masses of the holes, m_i, which show weak dependence on the Hall concentration, n_R, owing to the non-parabolicity of the valence band (see Table 3.1.4 and [Publication 1]). These parameters were used for the numerical interpretation of the anisotropy of the negative magnetoresistance in p-CdSb on the metallic side of the MIT using the approach presented in [52, 53].

The aim is to clarify the mechanisms of hopping conductivity discussed in Chapter 2.2 and connected to the nature of the charge carriers in the undoped p-CdSb. Special attention is given to the evolution of these effects and the anisotropy of the hopping conductivity in a magnetic field. These studies provide information on the critical behavior of microscopic parameters near the MIT and on the properties of the localized charge carriers.

Anisotropic quantum interference effects, such as weak localization and negative MR observed in the undoped p-CdSb [Publication 3] on the metallic side of MIT [52, 53], and the anisotropic hopping conductivity observed on the insulating side of the MIT, are in agreement with the anisotropy of m_i. Knowledge of the hopping charge transfer in this material is lacking, excluding an estimate of the mean localization radius of the holes ~ 100–170 Å in CdSb lightly doped with rare-earth elements [49].

In the present Chapter, the resistivity, the magnetoresistance and the Hall effect in wide temperature and magnetic field intervals in the undoped p-CdSb grown by the zone melting technique are investigated (see Chapter 2.3). These crystals were grown with the increased speed of the melting zone for the purpose to increase the concentration of acceptors without traditional doping. This means that the samples were “doped” by Cd vacancies.

The measurements of ρ (B,T) in all specimens were made in accordance with the procedure described in Chapter 2.3. MR measurements were made in transversal field configurations with $\boldsymbol{j} \parallel \boldsymbol{a}$ and $\boldsymbol{B} \parallel \boldsymbol{b}$; $\boldsymbol{j} \parallel \boldsymbol{a}$ and $\boldsymbol{B} \parallel \boldsymbol{c}$ (sample 1) and $\boldsymbol{j} \parallel \boldsymbol{b}$ and $\boldsymbol{B} \parallel \boldsymbol{a}$; $\boldsymbol{j} \parallel \boldsymbol{b}$ and $\boldsymbol{B} \parallel \boldsymbol{c}$ (sample 2).

The initial characterization of the samples could be made with the Hall effect measurements. Understanding of the temperature dependence of R_{Hall} in p-CdSb is not simple because of the presence of different kinds of charge carriers, namely holes in the two acceptor bands [12]. These carriers may be activated to the several, non-equivalent anisotropic valence band extrema [19, 37]. Therefore, Hall measurements give the acceptor concentration (cf. the corresponding data in [12, 19, 48]) only when the analyses of these results are combined with the analyses of MR data.

As shown in Fig. 3.1.7 for p-CdSb, a considerable difference of ρ (T) is observed in the measurements of the samples 1 (***j*** || ***a***) and 2 (***j*** || ***b***)**.** We can see that the variation of ρ (T) is relatively weak between 30–200 K but increases strongly when T is decreased below 30 K.

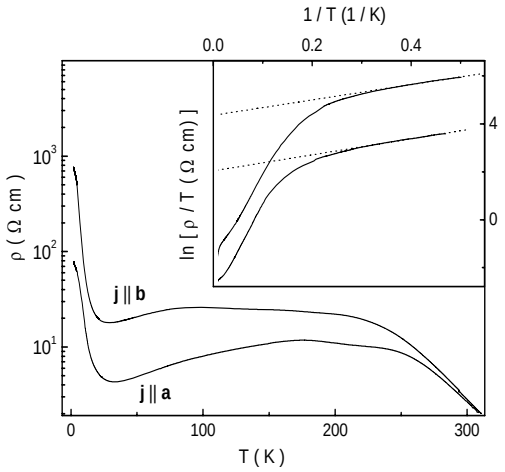

Figure 3.1.7**.** Temperature dependences of the resistivity of the undoped p-CdSb. The undoped samples for 1 (***j*** || ***a***) and 2 (***j*** || ***b***); the inset: plots of ln (ρ / T) vs. 1 / T. The dotted lines are linear fits.

The $\rho(B)$ dependence for p-CdSb is shown in Fig. 3.1.8 for different configurations of magnetic field. A large positive MR, increasing with the magnetic field and decreasing with the increasing of T is observed. However, a small negative MR with the maximum value of $\Delta \rho / \rho \sim 1$ % (see the inset to Fig. 3.1.8) is observed below $B \sim 1$–1.5 T, decreasing rapidly when the temperature is increased. A clear difference between the shapes of the ρ (T) curves measured in the samples 1 and 2 (upper and lower panels of Fig. 3.1.8, respectively) is clearly visible.

The R_H (B) dependences for p-CdSb shown in Fig. 3.1.9 for the samples 1 and 2 consist of a flat interval, broadening considerably with the increasing T, and degrading (?) behavior with the increasing B. The relative variation of both R_H (B) with B exhibiting maxima around $T \sim 6$–7 K is noted, while at T between 3.6–4.2 K and $B > 10$ T, an interval of increasing R_H (B) is observed. The shapes and values of R_H (B) at 4.2 K and $B < 2$–3 T are similar to those observed earlier in the undoped single crystals of p-CdSb [48].

Because of the wide range of magnetic fields, used in the study, the analysis of the experimental results obtained has to be done separately by low and high magnetic field approximations. The dependences of ln ρ vs. T^{-1} in zero magnetic field for the undoped p-CdSb exhibit several types of behavior (see the inset to Fig. 3.1.7).

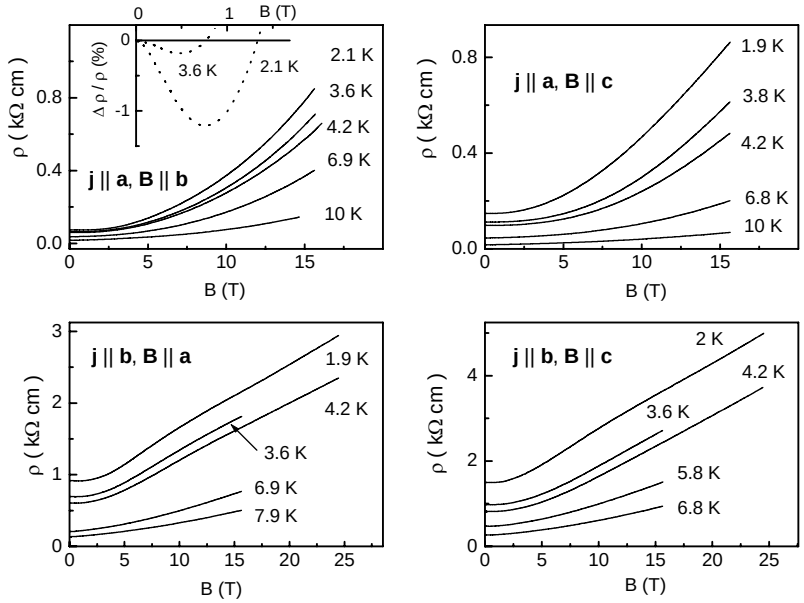

Figure 3.1.8. Dependence of the resistivity of p-CdSb on the magnetic field in the samples 1 (upper panels) and 2 (lower panels). The inset: the dependence of $\Delta\rho / \rho \equiv [\rho(B) - \rho(0)] / \rho(0)$ on B in the low field region.

As it is shown in the inset to Fig. 3.1.7, the dependences of ln (ρ/T) on $1/T$ in p-CdSb tend to linear functions with cooling. This corresponds to the transition to the NNH conductivity below $T \sim 5$ K according to Eq. (2.2.5). Calculations based on the slopes of the plots in the inset to Fig. 3.1.7 give $\varepsilon \approx 0.28$ meV and 0.30 meV for the samples 1 and 2, respectively. Therefore, the MR presented in Fig. 3.1.8 is analyzed by Eqs. (2.2.10–2.2.13).

The plots of ln ρ vs. B^2 in weak magnetic fields should be linear functions according to Eqs. (2.2.10–13) and their slopes should be independent of T. Such behavior is realized in the sample 1 (see Fig. 3.1.10) between $T = 3.6$–4.2 K below $B \approx 4.5$ T for $\boldsymbol{B} \parallel \boldsymbol{b}$ and between $T = 3.8$–4.2 K below $B \approx 7.5$ T for $\boldsymbol{B} \parallel \boldsymbol{c}$ (upper panels). Similar behavior

takes place in the sample 2 between T = 3.6–4.2 K below $B \approx 5.5$ T for $\boldsymbol{B} \parallel \boldsymbol{a}$ and below $B \approx 5.4$ T for $\boldsymbol{B} \parallel \boldsymbol{c}$ (lower panels).

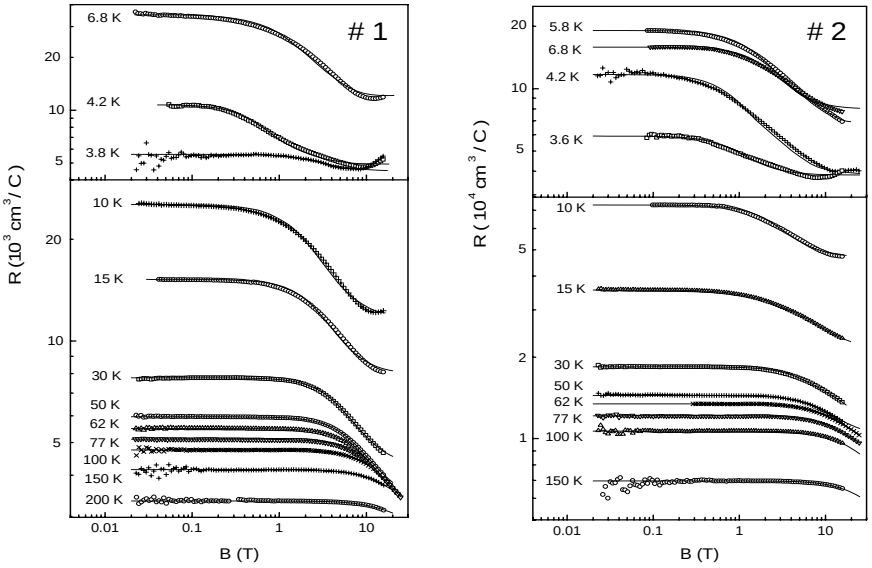

Figure 3.1.9**.** Dependences of the Hall coefficient on the magnetic field in the p-CdSb samples 1 and 2. The lines are fits to Eq. (2.2.16).

The deviations in the low fields are connected to the onset of the negative MR. For T < 3.6–3.8 K, the plots in all the panels of Fig. 3.1.10 can also be fitted using linear functions because of a possible contribution from the VRH conductivity. In this case, in low fields, MR has the same quadratic dependence of ln ρ vs. T^2 but with a slope increasing with lowering the temperature [54]. The deviations from the linearity with increasing temperature found above 4.2 K can be explained by the increasing of the conductivity because of thermal activation of the holes to the valence band from the shallow acceptor levels.

As follows from Eqs. (2.2.11) and (2.2.13), in the limit of strong fields, the linear plots of ln ρ vs. $B^{7/12}$ are expected, where the slopes should also be independent of T. The intervals of such behavior can be seen in Fig. 3.1.11, where the vertical dotted lines indicate the completion of the weak-field behavior in Fig. 3.1.10. It takes place between T = 2.1–6.9 K above $B \approx 4.5$ T for $\boldsymbol{B} \parallel \boldsymbol{b}$, and between T = 3.8–4.2 K above $B \approx 5.8$ T for $\boldsymbol{B} \parallel \boldsymbol{c}$ in the sample 1 (upper panels). In the sample 2, it happens between T = 7–8 K above $B \approx$ 4.8 T for $\boldsymbol{B} \parallel \boldsymbol{a}$ and between 4.2–6.8 K above $B \approx 4.9$ T for $\boldsymbol{B} \parallel \boldsymbol{c}$ (lower panels). Compared with the weak-field limit, the temperature intervals of the strong-field behavior

pertinent to the NNH conductivity are somewhat different, broadening in the sample 1 (for ***B*** || ***b***) and shifting to a higher temperature in the sample 2.

The appearance of the hopping conductivity at higher T in the strong magnetic field can be attributed to the increase of the energy of the shallow acceptor levels [Publication 3] and decreasing of the activation of the holes from the shallow acceptor levels to the valence band. However, a clear downward deviation from linearity (especially in the sample 2) in Fig. 3.1.11 with cooling suggests a pronounced contribution in strong magnetic fields from the VRH conductivity (having a weaker dependence on B than the NNH conductivity) [54]. The reason is that the impurity wave functions are strongly overlapping near the MIT, which decreases the value of ε, and the magnetic field weakens the overlapping by shrinking the wave functions, which can cause an additional increase in $\rho\,(B)$ with increasing ε.

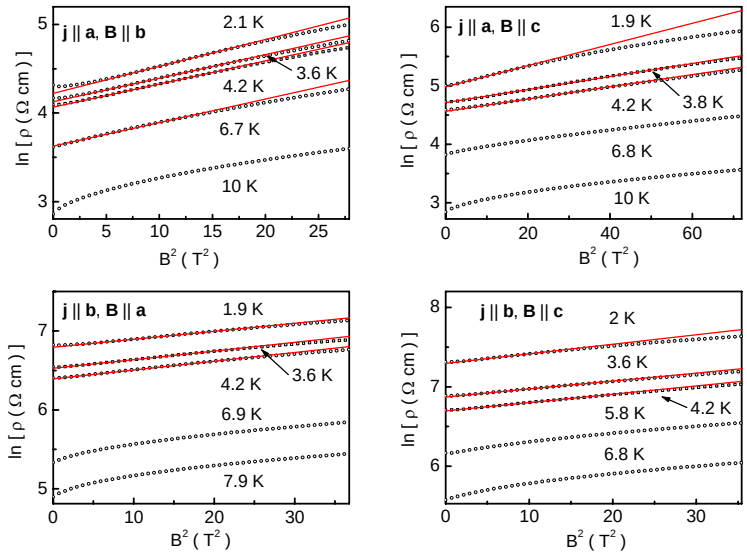

Figure 3.1.10**.** Plots for p-CdSb of ln ρ vs. B^2 for the sample 1 (upper panel) and the sample 2 (lower panel). The lines are linear fits to Eq. (2.2.11).

From the linear fits of the plots in Figs. 3.1.10 and 3.1.11, $C_{12} = 0.0264$, $C_{13} = 0.0108$, $C_{21} = 0.0111$, $C_{23} = 0.0103$ (in T^{-2}) and $S_{12} = 0.765$, $S_{13} = 0.625$, $S_{21} = 0.380$ and $S_{23} = 0.375$ (in $T^{-7/12}$) were obtained. For the same sample (the same first subscript), the ratios between the coefficients for different directions of the field (given by the second subscript) can be expressed through the ratios of the corresponding components of the effective mass, $C_{ij} / C_{ik} = m_j / m_k$ and $S_{ij} / S_{ik} = (m_j / m_k)^{7/24}$ with Eqs. (2.2.12–13). The

experimental and the calculated ratios agree within a few percents. Comparison the ratios of C_{ij} / C_{kn} and S_{ij} / S_{kn} for different samples ($i \neq k$) and different directions of $\boldsymbol{B}$ ($j \neq n$) with those calculated in [P3], C_{12} / C_{21} = 2.38 (2.29), C_{12} / C_{23} = 2.56 (2.62), S_{12} / S_{21} = 2.01 (2.09) and S_{12} / S_{23} = 2.04 (2.18), demonstrates an agreement within ~ 2–6 % [Publication 3].

The downward deviation of the plots in Fig. 3.1.11 is caused, most probably, by the transition to the VRH conductivity with lowering the temperature [Publication 3]. This supposition is proved by linear dependences of ln ρ vs. $B^{7/18}(T^{7/18})$, which is typical for VRH conductivity (see [Publication 3]) and are presented in Fig. 3.1.12.

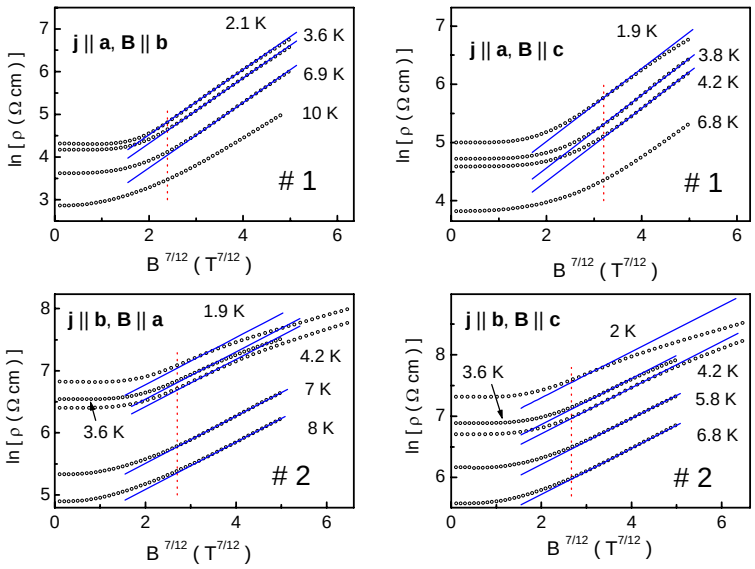

Figure 3.1.11. Plots for p-CdSb of ln ρ vs. $B^{7/12}$ for the sample 1 (upper panel) and the sample 2 (lower panel). The lines are linear fits of the data for $j \parallel a$, $B \parallel b$ between T = 3.6 – 6.9 K, for $j \parallel a$, $B \parallel c$ between T = 3.8 – 4.2 K, for $j \parallel b$, $B \parallel a$ between T = 7–8 K and for $j \parallel b$, $B \parallel c$ between T = 4.2 – 6.8 K to Eq. (2.2.11). The lines falling outside the given temperature regions are drawn parallel to the linear fits for comparison. The vertical dotted line marks the upper limit of the weak-field behavior in Fig. 3.1.14.

The evaluation of the values of the acceptor concentrations and the localization radii of the absolute values of the coefficients C_{12} and C_{21} is carried out in accordance with the Mott criterion for the MIT, $N_c^{1/3}a_0^* = \beta \approx 0.25$ [55, 56], in the analytical form for $\nu = 1$ (see [P3]). Finally, we obtain $N_c = 1.23\times10^{17}$ cm^{-3} and with Eq. (2.2.13) N_1 =

4.31×10^{16} cm^{-3}, $N_2 = 7.55\times10^{16}$ cm^{-3}. The values of a_0* are found to be the same within ~1 %, yielding a_0* = 50 Å.

The mean localization radii of the holes are a_1* = 78 Å in the sample 1 and a_2* = 126 Å in the sample 2 [Publication 3]. Because the impurity systems in both samples are sufficiently close to the MIT, the estimation of the localization radii with respect to that far from the MIT may be done as $a_0^*|_{calc} = \hbar / (2\, m^*\, E)^{-1/2}$ (see [P3]). Using the values of $m^* = (m_1 m_2 m_3)^{1/3} = 0.2\, m_0$ and $E = E_1 = 6.1$ meV for the lower acceptor level in undoped p-CdSb [8], we obtain $a_0^*|_{calc}$ = 56 Å in an acceptable agreement with a_0*= 50 Å found above.

The crossover fields estimated with Eqs. (2.2.8–9) and the relation $B_c' \approx 4\, B_c$ [Publication 3] are B_c = 3.0 T and 2.2 T, B_c' = 11.9 T and 8.9 T for the samples 1 and 2, respectively. The values of the fields between the end of the weak-field regime and the onset of the strong-field regime are lying inside the interval of (B_c, B_c') between ~ 4.5–7.5 T and ~ 4.8–5.4 T for the samples 1 and 2, respectively, and are presented above.

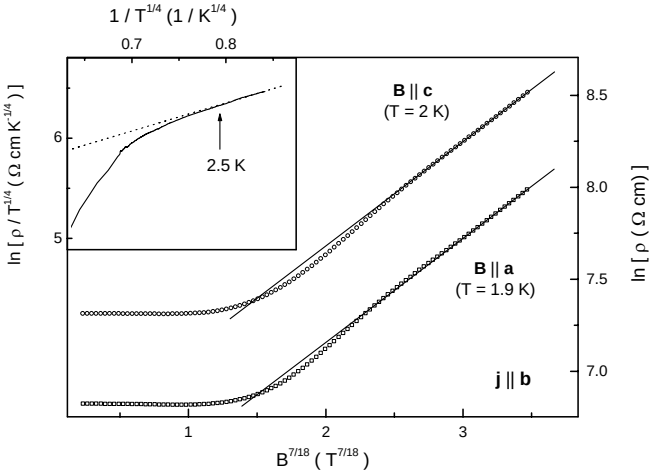

Figure 3.1.12. Plots for p-CdSb of ln ρ vs. $B^{7/18}$ in the sample 2. The solid lines are linear fits. The inset: the dependence of ln (ρ /$T^{1/4}$) on 1 / $T^{1/4}$, fitted with the linear fit (the dotted line) below 2.5 K.

The R_H (B) dependences for p-CdSb shown in Fig. 3.1.9 for the samples 1 and 2 consist of a flat interval, broadening considerably with increasing T, and descending behavior with increasing B, together with relative variation of both R (B) vs. B exhibiting maxima around T ~ 6–7 K. Increasing R_H (B) is observed at T between 3.6–4.2 K and B >

10 T. The shapes and the values of R_H (B) at 4.2 K and B < 2–3 T are similar to those observed earlier in undoped single crystals of p-CdSb [48].

The presented dependence of R_H on B (see Fig. 3.1.9) suggests a contribution of different groups of charge carriers. As mentioned in Chapter 2.2, these groups can be associated, generally, with the holes in the acceptor bands, A_1 and A_2, and with those thermally activated to various extrema of the valence band. The acceptor bands A_1 and A_2 have the energies $E_1^{(0)}$ and $E_2^{(0)}$ corresponding to the centres of the bands, the widths ΔE_1 and ΔE_2 and intervals of the itinerant states ΔE_{c1} and ΔE_{c2} around the band centres [62]. To simplify the analysis, the carriers are divided into the low- and high-mobile holes having the concentrations p_1 (T), p_2 (T) and mobilities μ_1 (T), μ_2 (T), respectively. This means that within any significant temperature interval, only two groups of the carriers with different concentration and mobility are assumed to contribute to R (T). The Hall effect is treated classically, restricting the analysis only to the itinerant carriers (including those in the A_1 and A_2 bands) and taking the Hall factor equal to unity.

As can be found from Fig. 3.1.9 (the solid lines), a good fit of R_H (B) with Eq. (2.2.15) is obtained for both samples 1 and 2 in a broad interval of temperature. Using R_0 and the values of R_∞ and μ obtained from the best fit of R_H (T) with Eq. (2.2.16), the functions p_j (T) and μ_j (T) (j = 1, 2) are evaluated (see [Publication 4]) and are shown in Fig. 3.1.13 for the sample 1. The character of dependences for the sample 2 is the same [Publication 4].

To analyze the data of p_j (T) (j = 1, 2), it is necessary to take into account the light-hole band, V_1, with the edge E_{V1}, consisting of two equivalent extrema of the valence band and having the DOS effective mass $m_1' = 2^{2/3}\, m_1$, where $m_1 = (m_a\, m_b\, m_c)^{1/3} \approx 0.20\, m_0$ [51–53]. The existence of a heavy-hole band, V_2, with the edge E_{V2} and the DOS effective mass $m_2 > m_1'$ should be supposed additionally. This is consistent with the increase of both functions p_j (T) with increasing T up to saturation as shown in Fig. 3.1.13. This behavior is connected to the thermal activation of the holes from the acceptor bands A_j followed by depletion of the acceptor states at high temperatures, and with the fact that p_2 exceeds p_1 including the interval of saturation. The difference $E_2^{(0)} - E_1^{(0)} = E_2 - E_1 \approx 3$ meV is comparable with the on-site Hubbard correlation energy, E_H, which for the hydrogen-like impurity wave function can be estimated as $E_H \approx 5\, e^2 / (8\, \kappa_0\, a) \sim 5$ meV [62].

Here the localization radius, a, determining the space decay of the impurity wave function, can be estimated with the Bohr radius $a_B = \hbar^2\, \kappa_0 / (m_1\, e^2) \approx 70$ Å and $\kappa_0 = (\kappa_{0a}\kappa_{0b}\kappa_{0c})^{1/3} \approx 25$ is the dielectric permittivity [57]. This points out that the acceptor bands

A_1 and A_2 in undoped p-CdSb can be considered as spin-split Hubbard-like bands, arising from the spin-degenerate local acceptor level due to the on-site Hubbard correlations [62], with the concentration of the acceptor states in each band equal to the concentration of the acceptor centres, N_A.

Therefore, at $T = 0$ only the upper acceptor band (A_2) can contain the holes with the concentration $N_A - N_D$, where $N_D = KN_A$ is the concentration of compensating donors and K is the degree of the compensation, while the lower acceptor band (A_1) and the valence bands V_1 and V_2 are empty. Taking into account the non-degeneracy of the valence bands and neglecting a weak non-parabolicity of the band V_1, the DOS function in each acceptor band may be approximated with a rectangular shape.

However, at this point, it has to be emphasized that no interval of the itinerant states can exist in a system of local impurity levels (since all local levels have the same energy), but only in an impurity band [62]. In the calculations, we used the values of E_1 and E_2 cited above and the values of $N_A \approx 4.3\times10^{16}$ cm^{-3} and 7.6×10^{16} cm^{-3}, which are relatively close to the critical concentration $N_c \approx 1.2\times10^{17}$ cm^{-3} as has been found in the investigations of the hopping conductivity in the same samples 1 and 2, respectively [see Publication 4].

By fitting the experimental data of p_2 (T) (see [Publication 4]) separately in the high- and low-temperature intervals, we obtain for the sample 1 $\Delta E_V \approx 0$, $m_2 \approx 0.75\ m_0$ and $\alpha_2 \approx 0.22$, respectively, and for the sample 2 $\Delta E_V \approx 1$ meV, $m_2 \approx 0.85\ m_0$ and $\alpha_2 \approx 0.09$, respectively. Figure 3.1.20 shows the concentrations of the itinerant holes in the bands A_2 (the dotted line, $\alpha_2\ p_{A2}$) and V_2 (the dashed line, p_{V2}) and their sum (the solid line, p_{2cal}), where the calculated curve reproduces well the experimental data.

The absolute values of ΔE_j and ΔE_{cj} were estimated by fitting the experimental data with the same curves as those shown in Fig. 3.1.13. The same values of the parameters m_2 and ΔE_V as obtained above were taken, giving $\Delta E_1 \approx 3$ meV, $\Delta E_{c1} \approx 0.7$ meV, $\Delta E_2 \approx 0.5$ meV and $\Delta E_{c2} \approx 0.12$ meV for the sample 1 and $\Delta E_1 \approx 4$ meV, $\Delta E_{c1} \approx 0.3$ meV, $\Delta E_2 \approx 0.5$ meV and $\Delta E_{c2} \approx 0.05$ meV for the sample 2.

An approximate analysis of the Hall mobility $\mu_R = R_0\ \rho^{-1}$ has been made by taking into account the optical phonon scattering with the result that this mechanism is not significant at temperatures below the Debye temperature $\theta = 180$ K [48]. Therefore, it is not included in the corresponding term in Eq. (2.2.16), which is accurate in the sense that it corresponds to the summation of the inverse relaxation times.

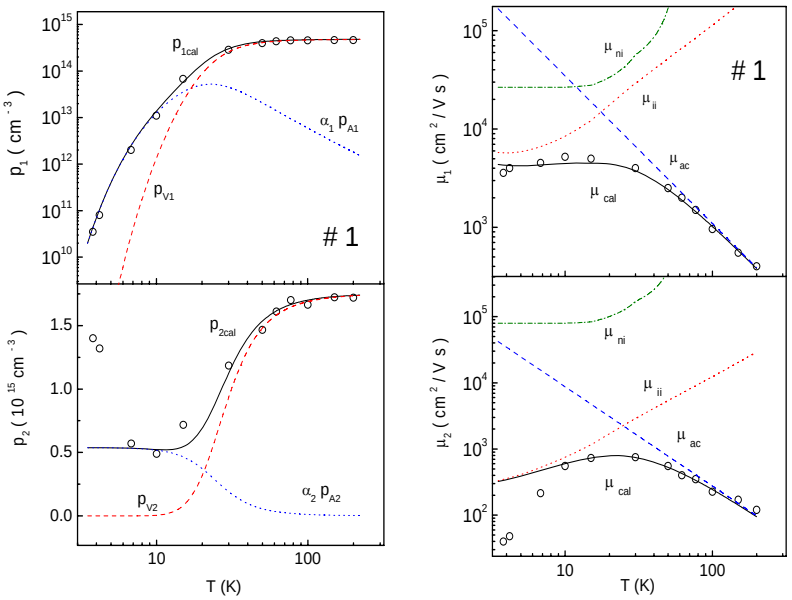

Figure 3.1.13. Dependence of p_1, μ_1 (the upper panels) and p_2, μ_2 (the lower panels) for p-CdSb on temperature in the sample 1 (O). The dotted lines for p_i are the contributions of the itinerant holes, $\alpha_1 p_{A1}$ and $\alpha_2 p_{A2}$, in the A_1 and A_2 bands, respectively, the dashed lines are the contributions of the holes p_{V1} and p_{V2} in the V_1 and V_2 bands, respectively, and the solid lines are their sums, p_{1cal}, evaluated with Eq. (11) from [Publication 4]. The dashed lines for μ_i are the contributions of the acoustic phonon scattering (μ_{ac}), the dotted lines are the contributions of the ionized impurity scattering (μ_{ii}), the dash-dot lines are the contributions of the neutral impurity scattering (μ_{ni}) and the solid line, μ_{cal}, is the total mobility evaluated with Eq. (2.2.16).

If the anisotropy of scattering can be neglected, the anisotropy of μ is determined only by the anisotropy of the effective mass of carriers. The components of the light-hole band effective mass m_j (cited in Chapter 3.1.2) were used to evaluate μ_1 (T) with Eq. (2.2.16) by changing $\mu \rightarrow \mu_j = (m_1 / m_j)\ \mu$ (j = a, b, c) and the DOS effective mass m_2 found in [Publication 4] to evaluate μ_2 with Eq. (2.2.16) directly. This means that the anisotropy of the light-hole band can be accurately taken into account. The same cannot be done with respect to the heavy-hole band (only the DOS effective mass is known), which is assumed to be roughly isotropic.

Figure 3.1.13 illustrates the contributions of μ_{ac} (the dashed line), μ_{ii} (the dot line), μ_{ni} (the dash-dot line) and the total mobility evaluated with Eq. (2.2.16) (the solid line,

μ_{cal}) for the sample 1. As can be expected, the acoustic phonon scattering and the ionized impurity scattering dominate in the high- and low-temperature intervals, respectively. At the same time, the contribution of the neutral impurity scattering to μ_I is small.

3.2 Electrical properties of n-CdSb at low temperatures in a magnetic field

3.2.1 Shubnikov–de Haas effect and energy band parameters in n-CdSb

So far, the n-type CdSb has not been investigated in such detail as the p-type because of difficulties in growing homogeneous single crystals. The SdH oscillations were observed in n-CdSb single crystals doped with In for the first time in this work, and are presented in Fig. 3.2.1. The anisotropy of the effect was investigated when the magnetic field was rotating in one of the perpendicular planes (100), (010) or (001) and in the planes formed by the directions [110]–[001] and [101]–[010]. A detailed study was necessary because of the contradictory data found in the literature on the anisotropy of the transport properties of n-CdSb and the models of the conductivity band (CB) structure.

The change in the period of the SdH oscillations was not more than 10% when magnetic field was rotating in the planes mentioned above, showing that the anisotropy of the Fermi surface of electrons is weak. Therefore, the following calculations with spherical approximation were chosen. The concentration of electrons participating in the SdH effect, n_{SdH}, was calculated with Eq. 2.1.11. The results are presented in Table 3.1.6.

The quantum oscillations of the Hall coefficient (OHC) in n-CdSb are also presented in Fig. 3.2.1; they were observed for the first time in CdSb during the present studies. The period of OHC is equal to the period of SdH oscillations, but OHC are shifted for half a period relative to the SdH oscillations towards the stronger magnetic fields. Only one period of oscillations is observed in the investigated n-CdSb samples, and no spin splitting effects are noticed.

The cyclotron effective masses of electrons on the Fermi level m_{nc} were estimated from the temperature dependence of the amplitudes of the SdH oscillations using Eqs. (2.1.19–2.1.20); the results are presented in Table 3.2.1. Table 3.2.1 shows the correlation between m_{nc} and the Fermi level E_F in the conduction band of CdSb. Hence, CB in this material is not completely parabolic.

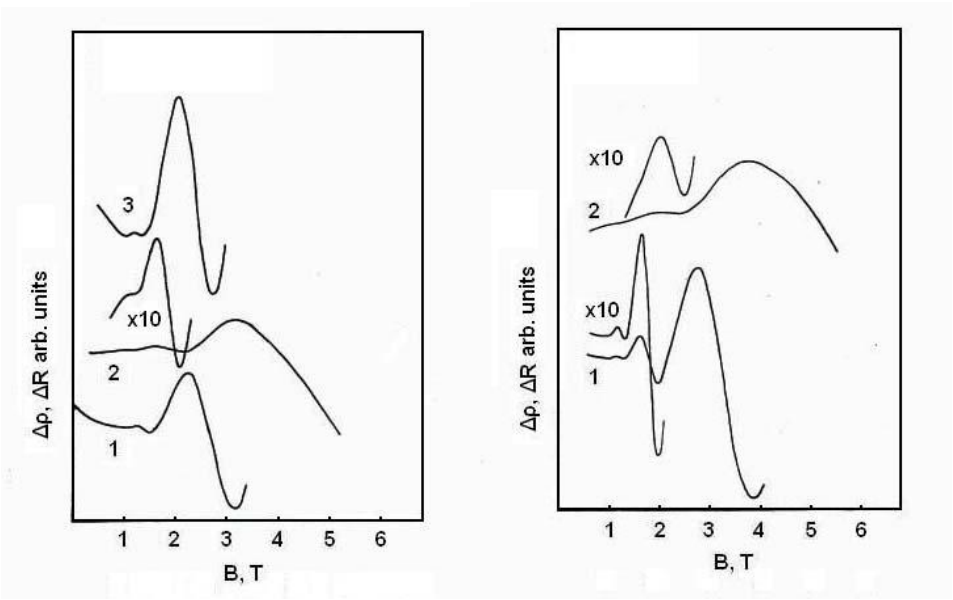

Fig. 3.2.1**.** SdH (curves 1, 3) and quantum oscillations of the Hall coefficient (curve 2) in the n-CdSb sample nA (left panel) and in the sample 101 (right panel) at T = 1.6 K. For better visibility, the low-field parts of the curves are amplified by the factor 10 (x10).

The CR measurements were performed in [31] on undoped p-CdSb samples under the illumination with energy higher than the CdSb band gap. This allows to assume that CR was detected on the electrons of the conduction band.

The estimation of the number of the equivalent valleys in the CB by the direct comparison of the Hall concentration estimated in a zero magnetic field, n_{R0}, and n_{SdH}, is not possible because of the large variation of the ratio n_{R0} / n_{SdH} from 6.5 to 8.5 for different samples (see Table 3.2.1). A possible reason is the second group of carriers, which have a higher effective mass and do not participate in the SdH effect, but participate in the Hall effect and the electrical conductivity.

The first argument for such an assumption lies in the fact that the Hall coefficient considerably depends on the magnetic field (see Table 3.2.1 and Fig. 3.2.2). The second argument is that the ratio $E_F / \hbar\omega_c$ is exactly equal to (N_m + ½) for all the SdH maxima including maxima with the small quantum numbers. This means pinning of the Fermi level by the neighboring energy band, because E_F does not depend on the magnetic field as it should in the case of one group of electrons. The third argument is that the OHC

phase is opposite to the SdH oscillations, and the amplitude of the OHC is notably higher than it is allowed by Eq. 3.1.5.

Table 3.2.1. Hall coefficient in zero magnetic field, R_0 , the Hall coefficient in infinite magnetic field, R_∞, specific conductivity, σ_0, concentration of electrons, calculated from the Hall coefficient in zero magnetic field, n_{R0}, period of the SdH oscillations, P_{SdH}, concentration of electrons participating in the SdH effect, n_{SdH}, cyclotron effective mass of electrons,m_{nc}, the Fermi energy, E_F, in n-CdSb at T = 4.2 K

SN	R_0 cm^3/C	R_∞ cm^3/C	σ_0 $Ohm^{-1}cm^{-1}$	n_{R0} 10^{17} cm^{-3}	P_{SdH} 10^{-2} T^{-1}	n_{SdH} 10^{17} cm^{-3}	$\frac{m_{nc}}{m_0}$	E_F meV
nA	44.0	27.2	122	1.42	40.5	0.22	0.10 ± 0.02	1.76
149	23.3	18.0	143	2.68	32.1	0.32	0.13 ± 0.02	2.13
101	19.0	15.1	252	3.29	27.8	0.39	0.16 ± 0.01	2.57
01	13.0	8.8	396	4.81	19.6	0.66	0.16 ± 0.01	3.38
200	8.1	4.9	620	7.72	14.8	1.1	0.17 ± 0.01	4.6
[31]	-	-	-	-	-	-	0.17 ± 0.01	-

Such behavior usually takes place when the nature of the OHC results from the real oscillating change in the carrier concentration in addition to the scattering process in a magnetic field, when the OHC take place because of the SdH oscillations of σ_{xx}^2 (see Eq. 3.2.1). The nature of such a phenomenon is the oscillating character of the density of states on the Fermi level versus the magnetic field, because the LLs are crossing the Fermi level (see Fig. 2.1.1). In the case of one group of carriers, their total concentration remains similar during the movement of the LLs across the Fermi level because electrons are moving to the lower LLs: the total density of states in the energy band under the Fermi level is constant and the OHC in this case are small.

The nature of the process is different if the Fermi level is located simultaneously in two energy bands with effective masses, and the carrier mobilities are so different that only one energy band is quantized. Thus, when some LL cross the Fermi level, the density of states in the quantized or “light” band is higher than in the non-quantized or “heavy” band, and the electrons move to it.

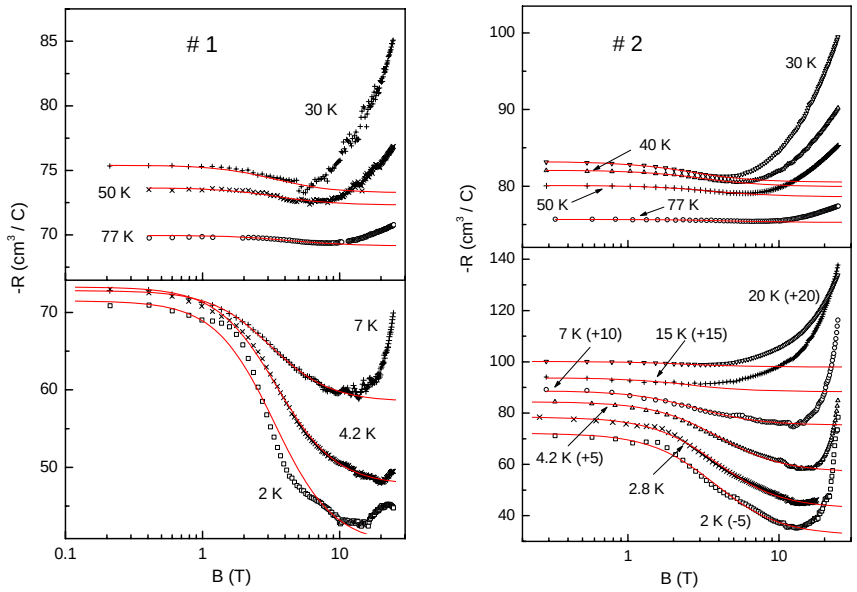

Fig. 3.2.2**.** Dependence of the Hall coefficient on the magnetic field in the n-CdSb samples nA1, the sample 1 (***j*** || [**010**]) and nA1, the sample 2 (***j*** || [**001**]) at different temperatures. For convenience, some of the data are shifted along the vertical axis by the values given in parentheses (in cm^3 / C).The lines are fits to Eq. 2.2.25.

When the Fermi level is in the "light" band between the LLs, the density of states is higher in the "heavy" band, and the electrons move to the "heavy" one. Because the main contribution to the Hall effect gives electrons with high mobility, their transfer to the "heavy" band results in high OHC because the concentration of "light" electrons really oscillates with the magnetic field.

3.2.2. Shallow impurity states and metal-insulator transition in n-CdSb

The investigations of the transport properties of In-doped n-CdSb in high magnetic fields were carried out using two types of sample configurations cut from the n-CdSb ingot grown by the zone melting technique (see Chapter 2.3). The sample 1 and the sample 2 have long edge parallel to the [**010**] and [**001**] axes, respectively. The Hall coefficient was determined in pulsed magnetic fields up to B = 25 T at constant temperatures between T = 2–77 K in transverse field configuration $\boldsymbol{B} \perp \boldsymbol{j}$ with ***j*** || [**010**] or [**001**], ***B*** || [**001**] or [**010**] axes for the samples 1 and 2, respectively.

The behavior of R (B) for the samples 1 and 2 shown in Fig. 3.2.2 consists of an almost flat interval, a descending part and an upturn, depending on T, when B is increased. The temperature dependence of R (B) exhibits a maximum between 7–30 K in the sample 1 and near 30 K in the sample 2, whereas the decrease in R (B) in the intermediate fields decays considerably with increasing T.

The reason for the above may be the second group of carriers, which have a larger effective mass than that proposed in Chapter 3.2.1. The group of the high-mobility itinerant carriers in n-CdSb can be associated with the electrons of CB participating in the SdH effect [77, Publication 2]. On the other hand, as follows from the discussion in Chapter 1.2, different models of CB in CdSb suggest an existence of several closely lying minima near the band edge. The temperature dependences of the carrier concentrations n_1 (T) and n_2 (T) and of their mobilities $\mu_1(T)$ and $\mu_2(T)$ were calculated with Eqs. (2.2.15–2.2.19) and they are presented in Figs. 4–7 in [Publication 5].

Dependences $n_1(T)$ and $n_2(T)$ were analyzed in the frame of a model of two groups of non-equivalent extrema of CB, characterized by different effective masses and mobilities of the electrons. The results of this analyses are evidently insufficient because of the temperature dependence of n_j (T) (j = 1, 2) having descending intervals below 20 K (see [Publication 5]). To account for the initial decrease with T of both functions n_1 (T) and n_2 (T), it is necessary to introduce an additional band with energy above the CB minima. Otherwise, all states of such a band would be occupied because of the location of the Fermi energy above the CB minima following from nonzero values of both n_j (T), j = 1, 2, at the lowest temperatures. This sub-band should have localized electron states, which can absorb itinerant electrons from the CB minima prohibiting them to participate in the classical Hall effect. Such a third band can be associated with the resonant impurity band (IB) containing only localized states. The performed calculations show [Publication 5] that this inconsistency is accompanied by an extremely large value of m_2 in the sample 1 with m_2/m_1 about 100. This is unphysical for conventional semiconductors. Therefore, it was concluded that the model including two groups of non-equivalent CB extremes and one IB with localized states is inconsistent.

A new analysis of n_1 (T) and n_2 (T) was based on another model of near-edge electron states. This model includes a single group of electrons from CB minima, C, with the DOS effective mass m and the concentration of the electrons n_c (T), and two Hubbard-like resonant IBs splitted by spin. These bands are I_1 with energy E_{i1} (T), total electron concentration n_{i1} (T), fraction $\alpha > 0$ of the delocalized states, concentration αn_{i1} (T) of the itinerant electrons, and I_2 with energy E_{i2} (T) containing only the localized states and the

concentration of (localized) electrons n_{i2} (T). The spectrum of DOS in this model at $T = 0$ and $B = 0$ is shown schematically in Fig. 3.2.4.

The best fit is obtained with fitting parameters collected in Table 3.2.2. The agreement between the experimental and calculated data is good (see Figs. 4–7 in [Publication 5]), excluding the lowest temperatures where it is worsening for both samples and both functions n_1 (T) and n_2 (T). However, this is attributable to a larger error of concentrations n_j (T) (j = 1, 2), determined with the two-band model, due to the oscillating contribution to R (B) at low T (see Fig. 3.2.1).

A pronounced difference of ρ (T) is observed between the samples 1 and 2, reaching an order of magnitude at the lowest temperatures as shown in Fig. 3.2.3.

An analysis of the mobility in undoped CdSb has demonstrated that scattering by the optical phonons is not significant at temperatures below ~ 200 K [5]. Therefore, the corresponding term in Eq. (2.2.16) was not included in the consideration. The contributions of the ionized impurities and the acoustic phonons enter Eq. (2.2.16) via the combined scattering term $1/\mu_{ac,ii}$, while the second term, $1/\mu_{ni}$, is substantiated because the relaxation time of the neutral impurity scattering does not depend on energy.

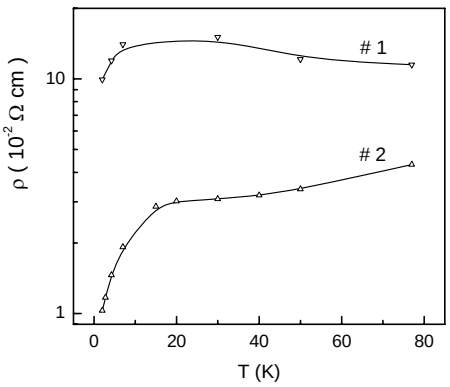

Figure 3.2.3. Temperature dependence of the resistivity in In the doped n-CdSb samples 1 and 2. The solid lines are to guide the eye.

The two IBs proposed above correspond to a possibility of adding two electrons with opposite spins on two levels of each impurity centre, with splitting ΔE_i approximately the on-site Hubbard correlation energy and the IBs appear due to broadening of each level [29]. The experimental data of μ_i (T) were fitted with Eq. (2.2.16) by treating A and D as

adjustable parameters, and the best fit was obtained with the values of A and D given in Table 3.2.2.

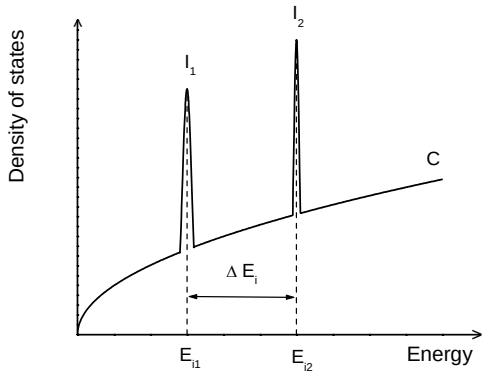

Figure 3.2.4. Density of states in CdSb near the CB edge vs. energy (schematically) at T = 0 and B = 0: C is CB and I_1 and I_2 are the spin-splitted IBs, having the maxima at E_{i1} and E_{i2}, respectively, and the energy difference ΔE_i.

The low-field interval was defined above so that neither parameters in Eq. (2.2.14) and, consequently, in Eq. (2.2.15) depend on B. Here is considered that fields $B > B_0$ where the condition $\mu B >> 1$ is satisfied and, additionally, R_∞ becomes a function of the magnetic field.

The latter may be connected to the following effects:

(i) shrinkage of the localization radius, a, of the electrons in the IBs by the field when the magnetic length λ becomes comparable with a, which leads to the magnetic field dependence of the impurity levels $\sim B^{1/3}$ in the interval $B_0 \le B \le 100\ B_0$ [30];

(ii) the fraction of the delocalized states in IB is determined by the degree of overlap of the impurity states which decreases when a is decreased [29], α also depends on the magnetic field at $B > B_0$;

(iii) the Zeeman shift of the spin-polarized impurity level, $\pm g\mu_B B / 2$, where g is the effective electron g-factor, becomes significant.

Here, the upturn of the Hall coefficient due to the effects listed above is analyzed. This is convenient for T > 20–30 K where the electrons occupy presumably the states of IBs. On the other hand, in this temperature interval, the electron gas is nondegenerate and we get $R_H(B) = \{1 + \exp[-\Delta E_i / (kT)]\} / [\alpha(B)\ e\ n_t(B_0)]$. In the ideal case, the parameter $n_t(B_0)$ should be close to n_t, the total concentration of the electrons, and the

parameter α does not depend on T (it is determined only by the overlap of the impurity states, which is insensitive to temperature).

Table 3.2.2. DOS effective mass, m, energy of the lower IB, E_i, temperature coefficient, β, energy difference between the IBs, ΔE_i, fraction of the delocalized states in the lower IB, α, concentration of the impurity centres, N_i, deformation potential for the acoustic phonons, D, scale factor, A, absolute value of the effective g-factor, $|g|$, total concentration of electrons, n_t, coefficient, ξ_1 ,of the $B^{1/3}$ contribution to E_{i1} (B) and ratio of the low-field localization radius and the mean distance between impurities, $a(B_0) / r_i$.

Sample No.	m/m_0	E_i meV	β meV/K	ΔE_i meV	α	N_i 10^{17} cm^{-3}	D eV	A	$\|g\|$	n_t 10^{17} cm^{-3}	ξ_1 $T^{-1/3}$	$a(B_0)$ / r_i
1	0.10	3.1	–0.47	0.9	1	5	25	20	1.11	1.56	–1.72	0.66
2	0.12	4	–0.38	0.9	0.63	1.6	25	1.05	1.35	2.34	–2.46	0.64

The functions $\alpha(B)$ at different temperatures were evaluated in [P5] for the cases when the Zeeman shift is omitted (see the insets to Fig. 3.2.5) and when it is taken into account (see the main parts of Fig. 3.2.5) by putting $B_0 = 9$ T. A strict analysis of the dependence $\alpha(B)$ is possible only for the hydrogenic impurities and shallow IB. Generally, the resonant IB does not satisfy these conditions [78], but the existence of the delocalized states in the I_1 suggests a large overlap of the impurity states, which for $N_i \sim 10^{17}$ cm^{-3} requires a large value of a comparable with a_B. This implies a certain similarity of the properties of impurity centres in n-CdSb case with the hydrogenic impurities. With the values of ξ_1 and $a(B_0) / r_i$ shown in Table 3.2.2, an agreement of the data in Fig. 3.2.5 was found with the functions calculated in [Publication 5] (solid lines) in the whole interval of $B \geq B_0$.

Investigations of $\rho(B)$ of n-CdSb show distinct dependence on magnetic field. The $\rho(B)$ isotherms shown in the main parts of Fig. 3.2.6 for the samples 1 and 2, exhibit a strong, exponential to the first approximation, dependence on B at low T, which decreases considerably with increasing temperature. Noticeable features of these data are the nonlinearity of the plots, especially for the sample 2, and crossing of all the plots at $B \sim 4$

T, excluding only that at T = 77 K (Fig. 3.2.6, right panel). The corresponding crossing of the ρ (T) plots for the sample 1 takes place in a notably narrower temperature interval between 2 and 7 K (Fig. 3.2.6, left panel).

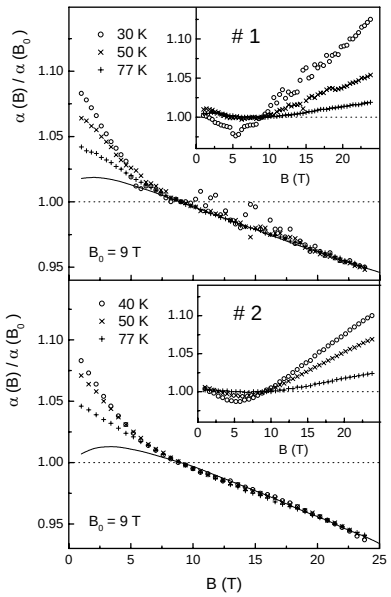

Figure 3.2.5**.** Dependence of α (B) / α (B_0) evaluated for n-CdSb with and without (insets) Zeeman shifts of the spin-splitted IBs for the sample 1 (upper panel) and the sample 2 (lower panel) at different temperatures. The solid line is evaluated with Eq. (21) from [Publication 5].

The insets to Fig. 3.2.6 show the dependences of ρ *(T)* in constant fields obtained from the plots in the main part of the figures. It is found that below $B \sim 4$ T, which is close to the crossing point of the ρ (B) curves, the low-temperature resistivity exhibits metallic behavior with $d\rho / dT > 0$. The metallic character of the resistivity in weak fields and $T \leq$ 4.2 K agrees with observation of the oscillating contribution to the Hall coefficient in both samples (see Fig. 3.2.1). However, above 4 T the sign of the derivative is changed, and with a further increase in the field, the resistivity demonstrates clear activated behavior characterized by exponential increase in ρ (T) when T is decreased. These features are characteristic of a metal-insulator transition (MIT) induced by a magnetic field, when a shift of the Fermi level, E_F, takes place from the interval of the extended states to that of the localized states in the electron energy spectrum [55, 62].

The details of the MIT in *n*-CdSb are discussed based on the model of near-edge electron states (see Fig. 3.2.4). In this case, ae dominating hopping charge transfer may take place over the localized states on the insulating side of the MIT [55]. According to the model [54] of the Mott VRH conductivity in the magnetic field, the resistivity can be presented in low fields ($B < B_c$) in the form of Eq. (2.2.6) and the crossover field by the Eqs (2.2.8–2.2.9).

The low-field behavior of the magnetoresistance for the sample 1 deviates from that of Eq. (2.2.6), exhibiting a clear curvature of the plots of ln ρ vs. B^2, together with a good linearity of these plots for the sample 2 between $T \sim 2$ and 7 K (see Fig. 3 in [Publication 6]). The deviation from the linear behavior with decreasing B is connected to approaching the MIT, while that with an increasing field is due to tending of B to B_c, where the values of B_c shown in the lower panel of Fig. 3.2.7 (circles) can be approximated with Eq. (2.2.9).

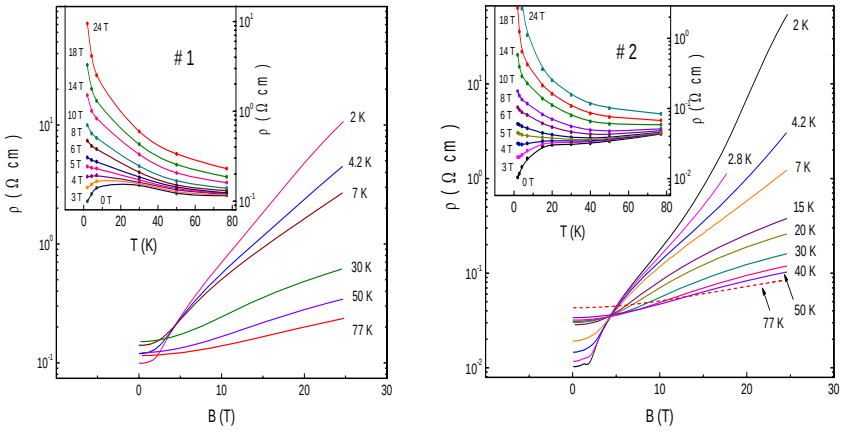

Figure 3.2.6. Dependences of the resistivity of n-CdSb on the magnetic field at constant T between 2–77 K in the sample 1 (left panel) and in the sample 2 (right panel). The insets: dependences of the resistivity on temperature in constant field B between 0–24 T for the same samples.

These behavior gives evidence for a power-law dependence of A (T) with exponent (– 0.80 ± 0.03), close to $T^{-3/4}$, whereas the plot of A vs. $T^{-3/4}$ exhibits a good linearity. Both plots lead to $C = (2.04 \pm 0.08) \times 10^{-2}$ T $^{-2}$ K $^{3/4}$.

The plots of ln ρ vs. $(B/T)^{1/3}$ for the sample 1 in the upper panel of Fig. 3.2.8 can be approximated by linear functions with the same slope, $\chi = 5.08 \pm 0.01$ K$^{1/3}$ T$^{-1/3}$, at T = 2.0, 4.2 and 7 K. Only the data at T = 30 K deviates from this tendency. Therefore, in the sample 1, the high-field asymptotic behavior of the magnetoresistance given by Eq. (2.2.6) is fulfilled above B_c, which depends on T close to prediction of Eq. (2.2.9), as can be seen in the lower panel of Fig. 3.2.7 (triangles). At the same time, for the sample 2, such plots demonstrate a divergence of the linear parts for different T (see the lower panel of Fig. 3.2.8).

Hence, the low-field asymptotic behavior of the Mott VRH conductivity is evident for the sample 2 and does not take place in the sample 1, whereas the high-field asymptotic behavior of $\rho(T, B)$ agrees with that of the Mott VRH mechanism only for the sample 1, but not for the sample 2. To clarify the reason of such a situation, the proposed above near-edge electron energy spectrum of *n*-CdSb at T = 0 K is taken into account (see Fig. 3.2.4). It is analyzed in two different intervals of the magnetic field, $B_0 < B < B_{cr}$ and $B > B_{cr}$, specifying the position of the Fermi level with respect to the bands I_1 and I_2.

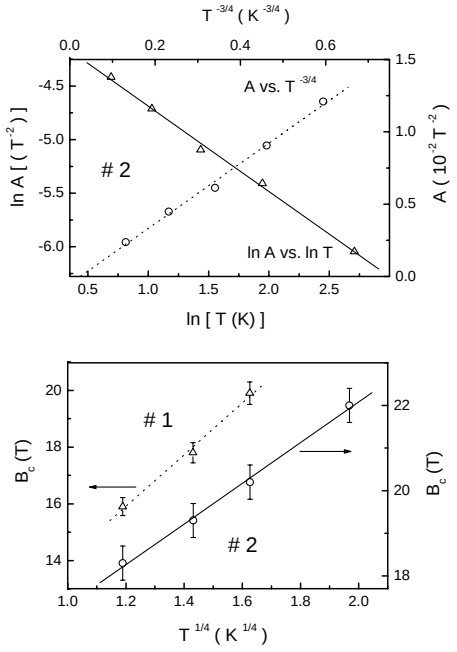

Figure 3.2.7. Plots of ln A vs. ln T (Δ) and A vs. $T^{-3/4}$ (○) in the sample 1. The lines are linear fits (upper panel). Dependences of B_c on $T^{1/4}$ in the sample 1 (Δ) and in the sample 2 (○). The lines are linear fits (lower panel).

In low fields, $B < B_0$, the clear two-band conductivity is evident in both samples from the decrease of the Hall coefficient (see Fig. 3.2.2) meaning that E_F lies in the interval of the extended states of I_1. As mentioned above, on the edges of the band I_1 of the sample 1 (which possesses only extended states in low fields) appear at $B > B_0$ intervals of localized states (the hatched areas in Fig. 3.2.9). Because $2N_i >> n_t$ in the sample 1 (see Table 3.2.2), the position of E_F will be always on the left edge of the lowest among the bands I_1 and I_2, independent of the position of the donor (D) band. Indeed, if the D band is above I_1 and I_2, then at $T = 0$ and $B > B_0$ it would be empty. In an opposite case, when the D band lies below I_1 and I_2 (as shown in Fig. 3.2.9) it has to be completely filled at $T = 0$. This happens because the amount of the allowed states below I_1 for $B > B_0$ is insufficient to transfer E_F from I_1 band to the D band due to absence of the CB states, which are shifted to the energies above those of I_1 and I_2. Therefore, the position of the completely filled D band below I_1 and I_2 in the sample 1 would lead only to an additional shift of E_F to the left edge of I_1, comparing with the cases of absence of the D band or with its position above I_1 and I_2.

The first consequence of the above consideration is that the magnetic-field induced MIT in the sample 1 takes place because of the appearance of the localized states at the left edge (or, more accurately, band tail) of I_1 around E_F. Here the case of $B > B_0 \sim 9$ T is discussed, whereas the change of the sign of the derivative $d\rho/dT$ in Fig. 3.2.6 takes place in smaller fields. This cannot contradict the proposed description because generation of the localized states in an impurity band is due to shrinkage of the impurity wave function, with the onset already at $B \sim B^* \sim 5$ T.

Because at $B_0 < B < B_{cr}$ E_F lies very close to the border between the localized and the extended states of I_1 (the mobility edge), another mechanism connected to thermal activation of the electrons from the states below E_F to the extended states of I_1 should make a comparable contribution to the conductivity. Therefore, in the sample 1 for $B_0 < B < B_{cr}$, the mechanism of mixed charge transfer takes place, which is the reason for the disagreement of the low-field MR (see upper panel in Fig. 3, [P6]) with that predicted for the pure VRH conductivity by Eq. (2.2.6).

As can be seen from the lower panel of Fig. 3.2.9, for $B > B_{cr}$ the band I_2 lies below I_1 and the same arguments as in the previous case show that E_F should lie in the left band tail of I_2. However, all states of I_2 are localized, and there is a larger energy difference between E_F and the extended states of I_1. This provides strong domination of the hopping conductivity mechanism at the lowest temperatures, and thus between 2–7 K the behavior

of the MR in strict accordance with Eq. (2.2.6) is observed violating it only at $T = 30$ K by the contribution of the electrons activated to the extended states of I_1.

In the sample 2, in low fields ($B < B_0$), E_F lies also in the interval of the extended states of I_1. Because in the sample 2 $N_i < n_t < 2N_i$ (Table 3.2.2), for $B_0 < B < B_{cr}$, E_F would lie in I_2 in the absence of the D band or in the case when it is above I_1 and I_2. If the D band lies below them, it would be completely filled at $T = 0$ because of the disappearance of the CB states, which have moved to energies above I_1 and I_2. However, in this case, no strong inequality exists between n_t and $2N_i$ (as in the sample 1), which allows E_F to lie within any interval of the localized states of the bands shown in the upper panel of Fig. 3.2.9, depending on the concentration N_d of the states in the D band.

The location of E_F in the left interval of the localized states of I_1 can be excluded; otherwise, the low-field asymptotic behavior of $\rho(T, B)$ will not be observed according to Eq. (2.2.6) because of the contribution of the itinerant electrons, activated from E_F to the extended states of I_1. If E_F lies among the interval of the localized states on the right-hand side of I_1 at $B_0 < B < B_{cr}$, then it would lie in I_2 relatively far from the extended states of I_1 at $B > B_{cr}$. In this case, there is (?) a low concentration of electrons in the extended states of I_1 at the lowest temperatures (the lower panel of Fig. 3.2.9) and allowing observation of the high-field asymptotic behavior of the magnetoresistance according to Eq. (2.2.6). Because quite an opposite picture is observed, a violation of the high-field VRH asymptotic behavior at $B > B_{cr}$ already between 2–7 K, the only possible position of E_F is that shown in Fig. 3.2.10, where the shift of E_F from the centre of the bands is tuned by the value of N_d.

On the other hand, because $B^* < B_0$, the magnetic-field induced MIT in the sample 2 is due to the transition of E_F from the interval of the extended states of I_1 to the interval of the localized states between the right mobility edge of I_1 and its position at $B \sim B_0$ in I_2 (the upper right panel of Fig. 3.2.9).

In such positions of E_F, the band I_1 is completely filled, excluding non-zero conductivity at $T = 0$ and permitting only negligible contribution to the charge transfer at low temperatures. Our results reflect the large overlap of the donor states, which is consistent with the observation of the low-temperature metallic conductivity in zero or a weak magnetic field. On the other hand, the fraction of the delocalized states in an impurity band is determined also by the degree of disorder, which increases with increasing impurity concentration and, therefore, in the sample 1, the disorder is also higher than in the sample 2 (see [Publication 6]).

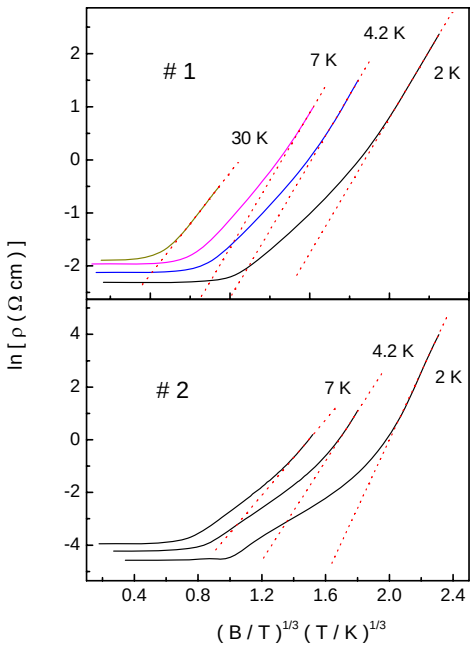

Figure 3.2.8. The plots of ln ρ vs. $(B / T)^{1/3}$ in the sample 1 (upper panel) and in the sample 2 (lower panel) for n-CdSb. The dotted lines are linear fits.

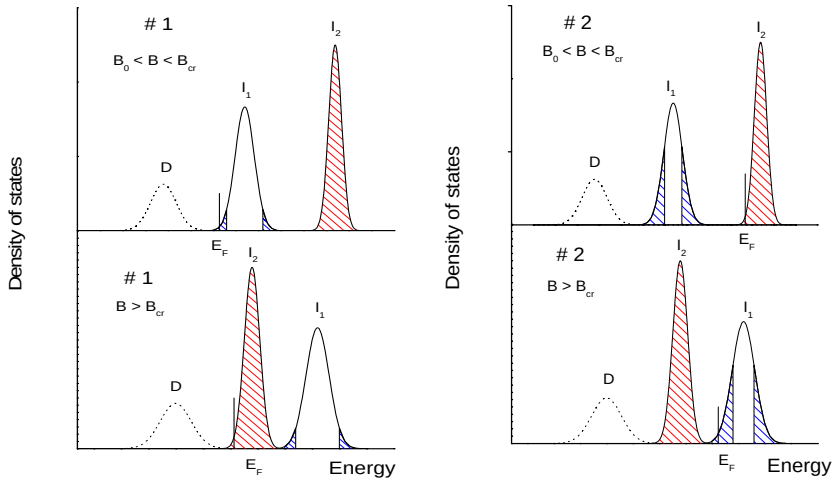

Figure 3.2.9. Density of states in CdSb near the CB edge vs. energy in the sample 1 (left panels) and in the sample 2 (right panels) at $T = 0$ in the magnetic field (schematically). The hatched areas represent the localized states.

Finally, observation of the VRH conductivity in our samples agrees with the position of E_F in the tail of I_2 (Fig. 3.2.10). Because at low temperatures the hopping is limited by the narrow energy interval around the Fermi level [55, 62], the mechanism of the NNH conductivity prevails when E_F lies near the peak of the impurity band [54], where DOS is large and the probability to find a neighboring impurity centre with an appropriate free level is high. On the other hand, in the band tail, the DOS is small and such a probability is strongly decreased, forcing the electrons to jump beyond the nearest neighbor sites, which leads to the VRH conductivity regime.

4 Conclusions

In this work, the results of the experimental investigations of the transport properties of the undoped CdSb and doped with shallow impurities such as In and Ag are presented with the aim to work out a correct model of the energy spectrum of this anisotropic semiconductor.

During these studies, Shubnikov–de Haas and the Hall coefficient oscillations in n- and p- type CdSb doped with In and Ag, respectively, are detected for the first time. Based on these experimental results, the shapes of the Fermi surfaces of electrons (sphere) and holes (ellipsoid) are estimated. Also the number of the equivalent extrema for the valence band (2), anisotropy coefficients, the components of the tensor of effective masses of carriers, *g*-factor and its anisotropy is determined. Nonparabolicity of the conduction and valence band is defined. The SdH experiments provided fundamental information allowing to deeply analyze the transport properties of the undoped CdSb and to work out a model for the energy spectrum near the bands edges in CdSb.

The investigations of the transport properties of undoped p-CdSb in weak and strong magnetic fields show that the anisotropy of the resistivity is determined completely by the anisotropy of the effective mass of the holes. The nearest-neighbor hopping conductivity regime is established below $T \sim 8$ K. Increasing deviations from the behavior pertinent to the NNH conductivity are observed by lowering the temperature and by increasing the magnetic field and the acceptor concentration, which are relatively close to the critical concentrations of the metal-insulator transition. Such behavior is attributable to the onset of the VRH conductivity regime.

At low temperatures, the existence of two groups of carriers, which are the itinerant holes in the upper and lower acceptor bands, was proven. At high temperatures, the carriers with the high and low mobility are the holes activated thermally to the light- and heavy-hole bands, respectively. Taking into account the contributions of the acoustic, ionized and neutral impurity scatterings, the analysis of the mobilities of carries supports the existence of two different valence sub-bands. These sub-bands are the anisotropic light-hole band and the approximately isotropic heavy-hole band, represented by an additional non-equivalent extremum of the valence band of CdSb with the measurably larger effective mass of holes.

The studies of galvanomagnetic effects in n-CdSb reveal the existence of two groups of carriers. These carriers are the electrons of a single minimum isotropic conduction band and the itinerant electrons of the narrow impurity band, having at low

temperatures energies above the bottom of the conduction band. It is found that above this impurity band, there exists another impurity band of only localized states, and the energies of both impurity bands depend on temperature so that they sink into the band gap when T is increased. These impurity bands are splitted by the spin. In strong magnetic fields, the energy difference between them decreases and redistribution of the electrons between the two impurity bands takes place.

The mobility of the conduction band carriers demonstrates that the scattering in n-CdSb at low temperatures is strongly anisotropic. This takes place because of the domination from scattering on the neutral impurity centres with increasing of the contribution to mobility from scattering by acoustic phonons when T increases. The metallic conductivity in zero or weak magnetic field is changed to activated conductivity by increasing B. Metal–insulator transition induced by the magnetic field takes place because of the shift of the Fermi level from the interval of extended states to that of the localized states of the electron spectrum near the edge of the conduction band. The Mott variable-range hopping conductivity is observed in the low- and high-field intervals on the insulating side of the MIT. The results yield information about the density of states and the localization radius of the resonant impurity band with completely localized states and about the donor band, which in high magnetic fields is separated from the conduction band and lies below the resonant impurity bands.

REFERENCES

1. M. Hansen, K. Anderko, *Structures of binary alloys* (Metallurgizdat, 1962).
2. N.A. Gorjunova, *Izv. AN SSSR, Phys*., **21**, 120 (1957).
3. L. Pauling, *Nature of the chemical bond* (Goshimizdat, 1947).
4. I.K. Andronik, M.V. Kot, *Sov. Solid State Phys*., **2**, 1128 (1960).
5. I.K. Andronik, M.V. Kot, *Izv. AN SSSR, Phys*., **28**, 1028 (1964).
6. I.K. Andronik, M.V. Kot, *Sov. Solid State Phys*., **3**, 2548 (1963).
7. V.P. Glushko, *Thermal constants of substances* (Nauka, 1973).
8. E. Mooser, W. Pearson, *Phys. Rev*. **101**, 492, (1956).
9. M. Miksovsky *et. al., Proc. of ICSP*, 1087 (1960).
10. K. Toman, Czech. *J. Phys*. **B, 13**, 431 (1963).
11. E.K. Arushanov, *Prog. Crystal Growth Charact*., **1**, 13 (1986).
12. S.M. Gusev, G.V. Rakin, *Sov. Solid State Phys*., **4**, 2328 (1962).
13. S.M. Gusev, *Izv. AN SSSR, Phys*., **28**, 1033 (1964).
14. A. Hruby, L. Stourac, *Czech. J. Phys*. B**, 14**, 130 (1964).
15. V.A. Stukan *et. al., Phys. Stat. Sol. (a)* **41**, 307 (1977).
16. I.K. Andronik, E.K. Arushanov, *Sov. Phys. Semicond*., **2**, 869 (1968).
17. S.M. Gusev, L.M. Zykin, *Sov. Phys. Semicond*., **7**, 780 (1973).
18. W.J. Turner, A.S. Fischler, W.E. Reese, *Phys. Rev*., **121**, 759 (1961).
19. T. Kawasaki, T. Tanaka, *J. Phys. Soc. Japan*, **21**, 2475 (1966).
20. L. Stourac, J. Tauc, M. Zavetova, *Proc. of ICSP*, 1091 (1960).
21. A.Hruby, J. Kubelic, L. Stourac, *Czech. J. Phys.* **B, 15**, 740 (1965).
22. M. Matias, A. Muller, *Czech. J. Phys.* **B, 16**, 106 (1966).
23. R. Smirous, A. Hruby, L. Stourac, *Czech. J. Phys*. **B, 13**, 350 (1963).
24. V.E. Kharciev, *Sov. Solid State Phys*., **4**, 983 (1962).
25. D.M. Bercha *et. al., Sov. Solid State Phys*., **12**, 2397 (1970).
26. V.E. Kharciev, *Sov. Solid State Phys*., **5**, 962 (1963).
27. A.Abraham, *Czech. J. Phys*. B**, 15**, 138 (1965).
28. F. Ermanis, E. Miller, *J. Electrochemical Soc*., **108**, 1048 (1961).
29. V. Frey *et. al., Proc. of ICSP*, 766 (1962).
30. M. Zavetova, *Czech. J. Phys.* **B, 14**, 615 (1964).
31. M.J. Stevenson, *Proceedings of Int Conf on the Physics of Semicond, Prague*, 1083 (1960).
32. M.J. Stevenson, *Bull. Amer. Phys. Soc*. S2, **5**, 177 (1960).

33. M. Matyas, *Czech. J. Phys*. **B, 17**, 227 (1967).
34. M. Zavetova, V. Vorlicek, *Czech. J. Phys*. **B, 19**, 677 (1969).
35. J. Tauc, A. Abraham, *Czech. J. Phys.* **B, 15**, 730 (1965).
36. B.P. Rheinlander, *Phys. Stat. Sol*., **38**, 193 (1970).
37. K.D. Tovstyuk *et. al., Phys. Stat. Sol*., **13**, 207 (1966).
38. Y. Yamada, *J. Phys. Soc. Japan*, **35**, 1600 (1973), **37**, 606 (1973).
39. D.M. Bercha, I.V. Slipukhina, M. Sznajder, and K.Z. Rushchanskii, *Phys. Rev*. **B**, **70,** 235206 (2004).
40. H. Komija, K. Masumoto, H. Fan, *Phys. Rev*., **133**, 1679 (1964).
41. L.D. Landau, E.M. Livshic, *Quantum mechanics* (Physmatgiz, 1963).
42. E.M. Livshic, A.M. Kosevich, *JETP*, **29**, 730 (1955).
43. I.M. Cidilkovsky, *Energy band structure of semiconductors* (Nauka, 1978).
44. Lazarev V B, Shevchenko V Ya, Grinberg Ya H, Sobolev V V 1978 *Semiconductor compounds of the II-V group* (Moscow: Nauka)
45. Gelich A M and Pilat I M, *Inorganic Mater.* **36** 330 (2000)
46. Semizorov A F, *Inorganic Mater.* **34** 770 (1998)
47. Ashcheulov A A and Gutsul I V, *J. Opt. Technol.* **67** 281 (2000)
48. Matsunami H, Nishihara Y and Tanaka T *J. Phys. Soc. Japan* **27** 1507, (1969)
49. Arushanov E K, Lisunov K G, Roznovan Yu V and Shubnikov M L, *Sov. Phys. Semicond*. **24** 744 (1990)
50. Andronik I K, Arushanov E K, Emelyanenko O V and Nasledov D N, *Fizika i Technika Poluprov.* **2** 1248 (1968)
51. , Cisowski J, Portal J-C, Arushanov E K, Broto J M, Huant S, and Brunel L C, *Phys. Stat. Sol. (b)*, **121**, 289 (1984).
52. Arushanov E K, Lashkul A V, Lisunov K G, Parfen'ev R V and Radautsan S I, *Sov. Phys. Solid State* **28** 1334 (1986)
53. Arushanov E K, Lashkul A V, Lisunov K G, Parfen'ev R V and Radautsan S I, *Sov. Phys. Solid State* **29** 1450 (1987)
54. Shklovskii B I and Efros A L, *Electronic Properties of Doped Semiconductors* (Berlin: Springer-Verlag) (1984)
55. Mott N F, *Metal-Insulator Transitions* (London: Taylor and Francis) (1990)
56. Castner T G, *Hopping Transport in Solid* ed. M Pollak and B Shklovskii (Amsterdam: Elsevier) p 3 (1991)

57. Borets A M, Rarenko I M and Rusnak V V 1984 *Proceedings of the 6th All-Union Joint Conf. on Materials Science of II-V Semiconductor Compounds* (Moscow: IONH) p 108
58. Stukan V A, Marenkin S F, Trifonov V I and Shevchenko V Ya, *Phys. Stat. Sol. (a)* **39** 445 (1977)
59. Chambers R G, *Proc. Phys. Soc* A **65** 903 (1952)
60. Radautsan S I, Arushanov E K, Nateprov A N and Chuiko G P, *Cadmium Arsenide and Phosphide* (Kishinev: Shtiintsa) p 29 (1976)
61. Arushanov E K and Chuiko G P, *Phys. Stat. Sol. (a)* **17** K135 (1973)
62. Mott N F and Davies E A, *Electron Processes in Non-Crystalline Materials* (Oxford: Clarendon) (1979); Mott N F, *Metal-Insulator Transitions* (London: Taylor and Francis) (1990)
63. Dornhaus R and Nimtz G, *Solid-State Physics: Springer Tracts in Modern Physics vol 78* ed G Höhler (Berlin: Springer-Verlag,) p 1 (1976)
64. Blakemore J S, *Semiconductor Statistics* (Oxford: Pergamon Press) (1962)
65. Seeger K, *Semiconductor Physics: Springer Series in Solid-State Science vol 40* (Berlin: Springer-Verlag) (1985)
66. Anatychyuk L M, Iskra V D, Rarenko I M and Sharlai B M, *Fizika Tverdogo Tela* **10** 3419 (1968)
67. Matyas M and Kiegl M, *Czech. J. Phys*. B **18** 356 (1968)
68. Marenkin S F, Saidullaeva M, Sanygin V P, and Kovaleva I S, *Izv. Akad. Nauk SSSR, Neorg. Mater.* **18** 1759 (1982)
69. Laiho R, Lashkul A V, Lisunov K G, Lähderanta E, Ojala I and Zakhvalinskii V S 2006 *Semicond. Sci. Technol*. **21** 228
70. Laiho R, Lashkul A V, Lisunov K G, Lähderanta E, Ojala I and Zakhvalinskii V S, *J. Magn. Magn. Mater.* **300** e8 (2006)
71. Shklovskii B I, *Sov. Phys. - Semicond*. **17** 1311 (1983)
72. Lisunov K G, Arushanov E, Vinzelberg H, Behr G and Schumann J, J. Appl. Phys. **97** 093706 (2005)
73. Arushanov E, Lisunov K G, , Vinzelberg H, Behr G and Schumann J, J. Appl. Phys. **100** 113704 (2006)
74. Dietl T, *Semimagnetic Semiconductors and Diluted Magnetic Semiconductors* ed. by M Averous and M Balkansky (New York, Plenum Press) (1991)
75. Anatychuk L I, Luste O Ya, Rarenko I M and Yaremiichuk B S, *Ukrain Fiz. Zhurnal* **15** 1216 (1970)

76. Danilevich O I, Ivanchuk R D and Rarenko I M, *Fizicheskaya Electronika* **10** 38 (1975)

77. Lashkul A V, Mashovets D V and Pruglo V I, *Proceedings of the 4th All-Union Conf. on Ternary Semicond. and Their Applications* (Kishinev: Shtiintsa) p 195 (1983)

78. Ravich Yu I and Nemov S A, *Semiconductors* **36** 1 (2002)

79. Erginsoy C, *Phys. Rev*. **79** 1013 (1950)

80. Hoo K and Becker W, *Phys. Rev*. B **14** 5372 (1976)

81. Honig A and Maxwell R, *Proceedings of the 9th International Conf. On the Physics of Semiconductors* (Leningrad: Nauka) p 1117 (1968)

82. Leotin J, Goiran M, and Askenazy S, *Phys. Stat. Sol. (b)*, **123**, K43 (1984).

83. Singh M, Wallace P R, Jog S D, and Arushanov E, *J. Phys. Chem. Solids,* **45** 409 (1984)

84. Leotin J, Goiran M, Askenazy S, Von Ortenberg M, Wallace P R, and Arushanov E, *Proceedings of the 17th Int Conf on the Physics of Semicond,* (Springer-Verlag, New York, NY, USA) p. 1021 (1985)

85. Goiran M, Zwick A, Carles R, Leotin J, Arushanov E, and Von Ortenberg M, *Phys. Stat. Sol. (b)*, **133** K1 (1986)

86. Martin J L, Goiran M, Arushanov E K, Leotin J, and Askenazy S, *Physica* **B 177** 481 (1992)

87. Singh M, *Phys. Rev.* **B 35** 9714 (1987)

Summary of the publications

The dissertation is based on the following six articles published in international journals.

Publication 1. E. K. Arushanov, A. V. Lashkul, V. I. Pruglo, S.I. Radautsan, V. V. Sologub, Shubnikov- de Haas oscillations in p-CdSb, Doklady Akademii Nauk SSSR **263**, 1, 71-73 (1982), (in Russian); Sov. Phys. Doklady (USA) **27**, 3, 212-3 (1982).

In this work, the Shubnikov–de Haas oscillations are detected for the first time in p-CdSb. Single crystalline samples are grown by zone melting technique and doped with Ag. The Shubnikov–de Haas effect is studied at the temperatures of 1.6 K–4.2 K in magnetic fields up to 7 T with different relative configurations of electric current and magnetic field. It is shown for the first time that the Fermi surface of holes in CdSb consists of two equivalent ellipsoids of general shape. The coefficients of anisotropy of the Fermi surface, the components of the tensor of the effective masses of the carriers, *g*-factor and its anisotropy are estimated during these studies. Nonparabolicity of the valence band is defined.

The Author of this dissertation carried out all the measurements, analyzed the obtained experimental data, made all the calculations, participated in the discussions and wrote the paper.

Publication 2. E. K. Arushanov, A. V. Lashkul, V. I. Pruglo, S.I. Radautsan, V. V. Sologub, Shubnikov- de Haas oscillations in n-CdSb, Doklady Akademii Nauk SSSR **263**, 5, 1112-14 (1982), (in Russian); Sov. Phys. Doklady (USA) **27**, 4, 320-321 (1982).

In this work, the Shubnikov–de Haas oscillations are detected for the first time in n-CdSb. Single crystalline samples are grown by zone melting technique and doped with In. The Shubnikov–de Haas effect is studied at the temperatures of 1.6 K–4.2 K in magnetic fields up to 7 T with different relative configurations of electric current and magnetic field. The studies of the galvanomagnetic effects in n-CdSb show the existence of two groups of electrons participating in conductivity, but only one group (“light” electrons) participates in the Shubnikov–de Haas effect. During these studies, it is shown for the first time that the Fermi surface of “light” electrons in CdSb has spherical symmetry, and their cyclotron mass is estimated. Nonparabolicity of the conduction band is defined.

The Author of this dissertation carried out all the measurements, analyzed the obtained experimental data, made all the calculations, participated in the discussions and wrote the paper.

Publication 3. R. Laiho, A. V. Lashkul, K. G. Lisunov, E. Lähderanta, M. O. Safonchik and M. A. Shakhov, Observation of the anisotropic hopping conductivity of p-CdSb in a magnetic field, J. Phys.: Condens. Matter **16,** 333-342 (2004).

The magnetoresistance of *p*-CdSb was investigated between T = 1.9–10 K in pulsed magnetic fields up to B = 25 T in a transversal magnetic field configuration, using undoped single crystal samples oriented along the directions [100] or [001]. The dependence of the resistivity on the direction of the magnetic field with respect to the crystallographic axes is observed. The anisotropy of the resistivity in weak and strong fields is determined completely by the anisotropy of the effective mass of the holes. The nearest-neighbor hopping conductivity regime is established below $T \sim 8$ K. Increasing deviations from the behavior pertinent to the NNH conductivity are observed with lowering the temperature and with increasing the magnetic field and the acceptor concentration. Such behavior is attributable to onset of the VRH conductivity regime.

The Author of this dissertation planned this work, analyzed the experimental data and participated in carrying out the measurements, discussions and writing the paper.

Publication 4. R. Laiho, A. V. Lashkul, K. G. Lisunov, E. Lähderanta, M. O. Safonchik and M. A. Shakhov, Hall effect and band structure of p-CdSb in strong magnetic field, Semicond. Sci. Technol. **19,** 602-609 (2004).

The Hall effect is investigated in undoped *p*-CdSb in a wide temperature interval in pulsed magnetic fields up to 25 T. The dependence of the Hall coefficient on B exhibits in low fields a flat region, followed by a descending interval when B is increased. The analysis of the Hall coefficient dependence versus magnetic field reveals an existence of two groups of the carriers with different concentration and mobility. The temperature dependence of the concentration of carriers contributing to the Hall effect demonstrates that at low temperatures the low- and high-mobile carriers are the itinerant holes in the upper and lower acceptor bands, respectively. At high temperatures, the carriers with the high and low mobility are the holes activated thermally to the light- and heavy-hole bands,

respectively. The analysis of the mobilities of the carries, taking into account the contributions of the acoustic, ionized and neutral impurity scatterings, supports the existence of the anisotropic light-hole band and the approximately isotropic heavy-hole band, represented by an additional non-equivalent extremum of the valence band of CdSb.

The Author of this dissertation planned this work, analyzed the experimental data and participated in carrying out the measurements, discussions and writing the paper.

Publication 5. R. Laiho, A. V. Lashkul, K. G. Lisunov, E. Lähderanta, M. O. Safonchik, M. A. Shakhov, The Hall effect and electron energy spectrum near the conduction band edge of n-CdSb in magnetic fields up to 25 T, Semicond. Sci. Technol. **21**, 918–927 (2006).

The Hall effect in In-doped *n*-CdSb was investigated at temperatures between $T = 2–77$ K in pulsed magnetic fields up to 25 T. The analysis of the Hall coefficient magnetic field dependence $B < B_0$, where $B_0 \sim 9$ T, reveals an existence of two groups of carriers with different concentrations and mobilities. The temperature dependence of the concentration of the carriers contributing to the Hall effect demonstrates that the high-mobility carriers are the electrons of a single minimum isotropic conduction band, whereas the low-mobility carriers are the itinerant electrons of the narrow impurity band, having at low temperatures the energies above the bottom of the conduction band. Above this impurity band, there exists another impurity band of only localized states. The energy of both impurity bands depend on temperature so that they sink into the band gap when T is increased. The bands are splitted by the spin, and in strong magnetic fields, the energy difference between them decreases leading to an increase in the Hall coefficient caused by the diminution of the concentration of the itinerant electrons by the redistribution of the electrons between the two impurity bands. The analysis of the mobility of the conduction band carriers, taking into account the contributions of the acoustic phonons, ionized and neutral impurity scattering mechanisms, demonstrates that scattering in *n*-CdSb is strongly anisotropic because of the domination of the contribution from neutral impurity centres.

The Author of this dissertation planned this work, analyzed the experimental data and participated in carrying out the measurements, discussions and writing the paper.

Publication 6. R. Laiho, A. V. Lashkul, K. G. Lisunov, E. Lähderanta, M. O. Safonchik, M. A. Shakhov, Metal-insulator transition and variable-range hopping conductivity of n-CdSb in magnetic field, J. Physics and Chemistry of Solids, **68,** 272-279 (2007)

The magnetoresistance of *p*-CdSb is investigated between T = 1.9–10 K in pulsed magnetic fields up to B = 25 T in a transversal magnetic field configuration, using undoped single crystal samples oriented along the directions [100] or [001]. The dependence of the resistivity on the direction of the magnetic field with respect to the crystallographic axes is observed. The anisotropy of the resistivity in weak and strong fields is determined completely by the anisotropy of the effective mass of the holes. The nearest-neighbor hopping conductivity regime is established below $T \sim 8$ K. The values of the acceptor concentration are relatively close to the critical concentrations of the metal-insulator transition. The average localization radii are enhanced with respect to that expected far from the metal-insulator transition and determined by the asymptote of the wave function far from the impurity centre. Increasing deviations from the behavior pertinent to the NNH conductivity are observed with lowering the temperature and with increasing the magnetic field and the acceptor concentration. Such behavior is attributable to the onset of the VRH conductivity regime. Additional investigations at lower temperatures are needed before a final conclusion about the type of the VRH regime is possible.

The Author of this dissertation planned this work, analyzed the experimental data and participated in carrying out the measurements, discussions and writing the paper.